Introductory Lecture

Oxide surfaces

Hans-Joachim Freund

Fritz-Haber-Institut der Max-Planck-Gesellschaft, Department of Chemical Physics, Faradayweg 4-6, D-14195 Berlin, Germany

Received 6th September 1999

Oxides have gained increasing interest in surface science during recent years because of their important role in applications. In the first part of the lecture we review the current knowledge on morphology and structure of surfaces of bulk single crystals as well as oxide films. The interaction of oxide surfaces with molecules is thoroughly discussed and the role of defects on adsorption is highlighted. In a further part, structure and morphology of deposited aggregates on clean and modified substrates are discussed. Such systems may serve as models for heterogeneous catalysts. Electronic structure as a function of the size of the deposited particle is studied, as well as size dependent adsorption properties and reactivities.

Introduction

The bulk properties of simple binary oxides are well understood and there are excellent reviews and text books available treating the various physical aspects.[1–5] In sharp contrast to the situation encountered for the bulk properties rather little is known about the surfaces of oxides, even the most simple ones. Only recently, if compared with the thirty years of surface science that have passed by,[6] researchers have started to study the surface science of oxides. There is a very useful book that marks a first milestone in this effort entitled "The surface science of oxides" by V. E. Henrich and P. A. Cox.[7] Since the publication of this book several reviews have appeared which have covered the field up to the present date.[8–15] It is understood that there are classes of oxides exhibiting external and internal surfaces, *i.e.* zeolites and meso-porous materials which are technologically very important. The present lecture will not discuss these even though some of the aspects which are dwelled upon here could be applied to those materials. We refer the reader to the paper of Thomas summarizing his Introductory Lecture of *Faraday Discussion* no. 105 where he discusses some aspects of this field as well.[16]

The present lecture has been organized as follows. In the first part we discuss several aspects of the geometric and electronic structure of clean oxide surfaces as determined by a variety of experimental methods. We show examples of surfaces terminating bulk single crystals as well as surfaces of epitaxial oxide films. This part is followed by examples attempting to illustrate some of the principles governing the interaction of molecules with oxide surfaces. A short comparison between the situation encountered on single crystalline surfaces with microcrystalline surfaces is included in order to demonstrate the influence of defects on the adsorption properties. The third part is dedicated to the interaction of metals with oxide surfaces and the study of deposited metal aggregates, including adsorption and reaction of molecules on such systems. Such composites represent

model systems for heterogeneous catalysts and allow us to try to bridge the material's gap between single crystal metal surfaces and real catalysts.[8–15,17–19] When a physical chemist talks about catalysis the situation is similar to a mathematician trying to convince engineers that what he does is of use for them. G. H. Hardy's *A Mathematician's Apology*, 1940, contains many useful thoughts on this problem.[20] One is:

> *It is one of the first duties of a professor, for example, in any subject, to exaggerate a little both the importance of his subject and his own importance in it. A man who is always asking 'Is what I do worth while?' and 'Am I the right person to do it?' will always be ineffective himself and a discouragement to others. He must shut his eyes a little and think a little more of his subject and himself than they deserve.*

Structure and adsorption on clean oxide surfaces

The preparation of a clean oxide surface is a rather difficult task. Several strategies have been followed.[7,21,22]

The most straightforward strategy is UHV *in situ* cleavage, which, however, only leads to good results in certain cases, such as MgO, NiO, ZnO, $SrTiO_3$, *etc.*[13] Some very interesting materials such as Al_2O_3, SiO_2, TiO_2, *etc.* are hard to cleave.[7] A disadvantage with respect to experimental investigations of cleaved bulk single crystal insulators is their low conductivity. An alternative way of bulk single crystal surface preparation is *ex situ* cutting and polishing followed by an *in situ* treatment by sputtering and subsequent annealing in oxygen. Through such a process a sufficient number of defects is created in the near surface region and in the bulk to support conductivity of the material. This leads to a situation where electron spectroscopies as well as STM can be applied.[7]

Single crystalline oxide surfaces may also be prepared *via* the growth of thin oxide films on single crystal metal supports.[11,21,22] To such systems all surface science tools can be applied without further problems. If the oxide film is supposed to represent the bulk situation special care has to be taken in the control of film thickness. Also, if adsorption and reactivity studies are intended the continuity of the film has to be guaranteed. There are several examples in the literature where this has been achieved.[10,11,23]

Probably, the best studied clean oxide surfaces are the $TiO_2(100)$ and $TiO_2(110)$ surfaces.[7,21,24] A STM image of the clean (1×1) $TiO_2(110)$ surface taken by Diebold and her group[25] is shown in Fig. 1. It is noteworthy that one of the first atomically resolved images of this surface was reported by Thornton and his group.[26,27] The inset shows a ball and stick model of the surface.

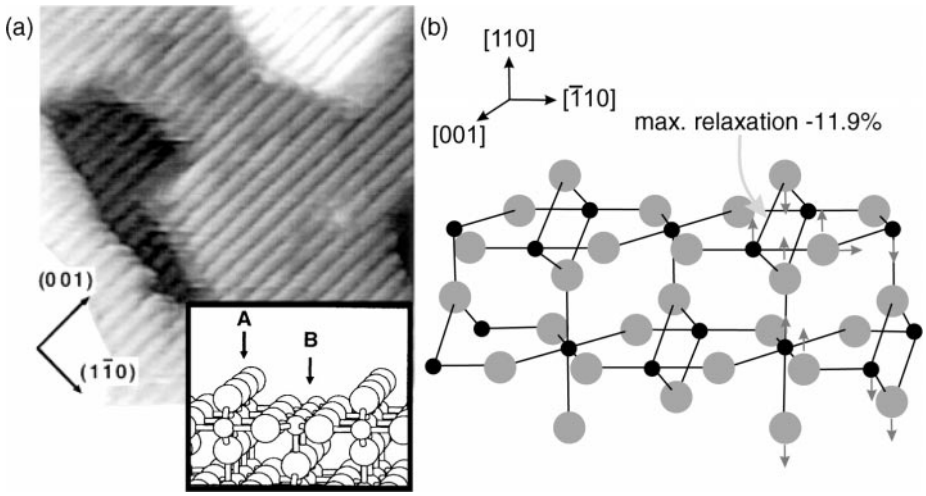

Fig. 1 Structure of the $TiO_2(110)$ (1×1) surface as determined *via* STM (a, reproduced from ref. 25) and grazing incidence X-ray scattering (b, adapted from ref. 32).

There is now accumulating evidence from theoretical modeling of the tunneling conditions, but also from adsorbate studies using molecules which are assumed to bind to the exposed Ti-sites, that the bright rows represent Ti atoms. Iwasawa and his group[28–31] have successfully used formic acid in such a study, and showed in line with the theoretical predictions, and counter-intuitive with respect to topological arguments, that the Ti ions are imaged as bright lines and the oxygen rows as dark lines. Taking the resolvable interatomic distances within the surface layer the values correspond to the structure of the charge neutral truncation of the stoichiometric (110) surface.[32] Interatomic distances normal to the surface, however, are substantially different from the bulk values as is revealed by X-ray scattering experiments.[32] The top layer six-fold coordinated Ti atoms move outward and the five-fold-coordinated Ti atoms inward. This leads to a rumpling of 0.3 ± 0.1 Å. The rumpling repeats itself in the second layer down with an amplitude of about half of that in the top layer. Bond length variations range from 11.3% contraction to 9.3% expansion. These strong relaxations are not untypical for oxide surfaces and had been theoretically predicted for quite a while.[33]

The relaxations are particularly pronounced for the so-called charge-neutralized polar surfaces.[34–36] There are several experimental results,[37–40] basically corroborating the theoretical predictions although the quantitative agreement is not always good.[41–44] Specifically, the (0001) surfaces of corundum-type materials such as Al_2O_3,[41,42] Cr_2O_3[43] and Fe_2O_3[44] have been studied with X-ray diffraction, quantitative LEED as well as with STM and theoretical methods. Fig. 2 reminds the reader briefly of the fact that a polar surface (*e.g.* (111) orientation for a rock-salt structure) exhibits, if bulk terminated, a diverging surface potential due to the missing compensation of the interlayer dipole moments, as is nicely discussed in Noguera's book.[36] Consequently, polar surfaces reconstruct and/or relax substantially, while non-polar surfaces often exhibit much less pronounced relaxations although, as shown above for TiO_2 the degree of relaxation is substantial. Fig. 3 shows the results of structural determinations for the three related

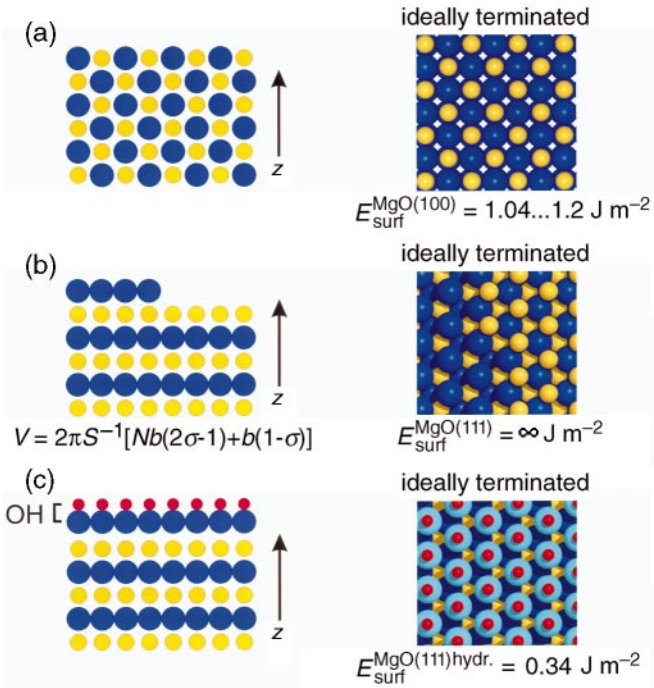

Fig. 2 Schematic representation (side and top views) of the structure of a non-polar (a, MeO(100), an unreconstructed polar (b, MeO(111)) and hydroxylated polar (c, MeO(111) adsorbate stabilized surface) surface of a rock-salt type crystal. The energies given refer to MgO.[177,178] (V, surface potential; S, area of surface unit cell; N, number of layers; b, interlayer spacing; σ, charge on surface layer relative to a layer in the bulk.)

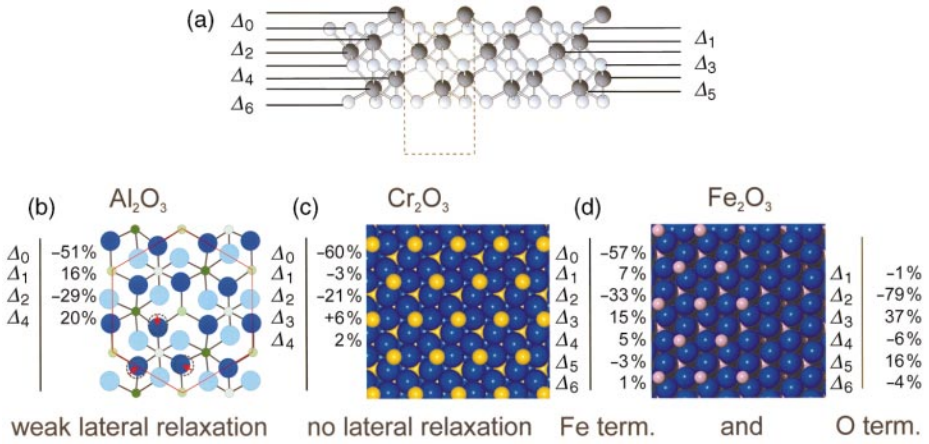

Fig. 3 Experimental data on the structure of corundum-type depolarized (0001) surfaces (side and top views). Adapted from (b) ref. 33; (c) ref. 39, and (d) ref. 44.

systems $Al_2O_3(0001)$, $Cr_2O_3(0001)$ and $Fe_2O_3(0001)$ as addressed above. In all cases a stable structure in UHV is the metal ion terminated surface retaining only half of the number of metal ions in the surface as compared to a full buckled layer of metal ions within the bulk. The interlayer distances are very strongly relaxed down to several layers below the surface. The perturbation of the structure due to the presence of the surface in oxides is considerably more pronounced than in metals, where the interlayer relaxations are typically of the order of a few percent.[45] The absence of the screening charge in a dielectric material such as an oxide contributes to this effect considerably. It has recently been pointed out[46] that oxide structures may not be as rigid as one might think judged on the relatively stiff phonon spectrum in the bulk. In fact, at the surface the phonon spectrum may become soft so that the geometric structure becomes rather flexible, and thus also very much dependent on the presence of adsorbed species.

Bulk oxide stoichiometries depend strongly on oxygen pressure, a fact that has been recognized for a long time.[47] So do oxide surfaces, structures and stoichiometries, a fact that has been shown again in a recent study on the $Fe_2O_3(0001)$ surface by the Scheffler and Schlögl groups.[44] In fact, if a Fe_2O_3 single crystalline film is grown in low oxygen pressure, the surface is metal terminated while growth under higher oxygen pressures leads to a complete oxygen termination.[44] This surface would be formally unstable on the basis of the electrostatic arguments presented above. However, calculations by the Scheffler group[44] have shown that a strong rearrangement of the electron distribution as well as relaxation between the layers leads to stabilization of the system. STM images by Weiss and co-workers[44] corroborate the coexistence of oxygen and iron terminated layers and thus indicate that stabilization must occur. Of course, there is need for further structural characterization. The idea of polar and non-polar surfaces only really holds in its simplest version as presented above if the material is very highly ionic. Thus, the most extreme cases to look at are perhaps the polar surfaces of the simple oxides with rock-salt structure[48] such as MgO and NiO, *i.e.* MgO(111) and NiO(111). Recently, Barbier *et al.*[49] have succeeded in preparing a single crystal NiO(111) surface, and to characterize it *via* grazing incidence X-ray diffraction (GIXD)! As was shown earlier for the case of thin NiO films of different crystallographic orientations, *i.e.* NiO(100)[50] and NiO(111),[51,52] a surface prepared in air or under residual gas pressure exhibits a $p(1 \times 1)$ structure while the clean polar (111) surfaces are reconstructed. The $p(2 \times 2)$ reconstruction originally reported for the thin film system has also been found for the bulk single crystal surfaces.[48,49] An initial structural analysis indicated that the actual structure is not the expected octopolar reconstruction shown in Fig. 4 but a more complicated one.[48] However, more recent investigations[53] of more carefully prepared bulk single crystal surfaces reveal that a stoichiometric surface actually reconstructs according to the octopolar scheme.[36,54] The small (100) terminated pyramids are oxygen terminated. Very recently, NiO(111) films grown on Au(111), which were initially studied by Neddermeyer and his group,[55] have been investigated

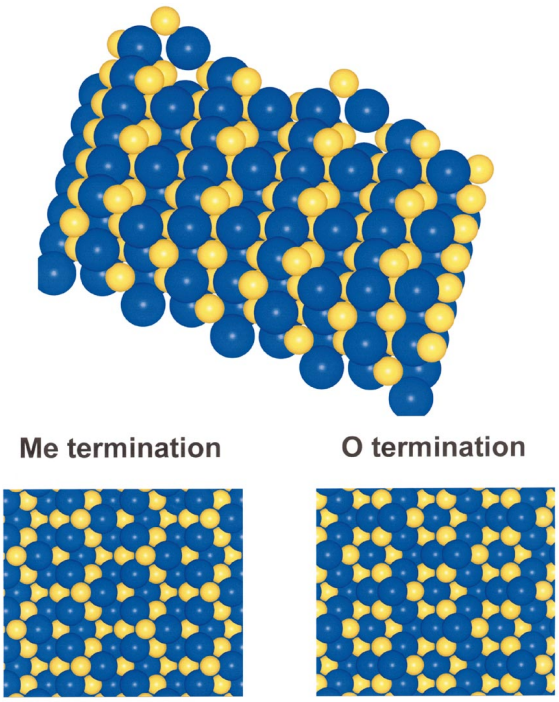

Fig. 4 Schematic representation of the octopolar reconstruction of a polar rock-salt (111) surface in oxygen and metal termination. Adapted from ref. 48.

by GIXD.[56] The p(2 × 2) reconstruction was again corroborated, but the structural analysis undertaken up to now would seem to favor a structure where oxygen as well as Ni-terminated octopols, possibly arranged on adjacent terraces constitute the surface layer. Both, the bulk single crystal surfaces as well as the NiO(111) film surfaces grown on Au(111) exhibit high degrees of surface order. This is probably one reason why these surfaces do not quickly restructure upon exposure to water, while NiO(111) films grown on Ni(111) do reconstruct to form a hydroxy terminated NiO(111) surface.[51,52] A microscopic mechanism would involve massive material transport across the surface, which is the more unfavorable the better the order, and may therefore be kinetically hindered on well ordered single crystals. We would like to note at this point that the interaction of water with polar oxide surfaces is a topic of general interest in geochemical and environmental issues[57] as well as in catalysis. With respect to the latter, Papp *et al.* have found indications that NiO catalysts prepared with preferential (111) crystallographic orientation by topotactical dehydration of $Ni(OH)_2$ do show the highest activity towards $DeNO_x$-reactions after the last monolayer of H_2O has been desorbed.[58,59] Already in 1977, Derouane and co-workers[60] had theoretically analyzed on the basis of energetic considerations that real crystallites must be terminated partly by polar surfaces whose charge has been reduced *via* OH adsorption.

It is thus evident that the general study of the interaction of molecules with oxide surfaces represents an interesting and important field of study. In the following we are going to discuss several examples in order to bring out certain aspects of the bonding and interaction of molecules with oxide surfaces. This will be discussed in comparison with the adsorption of molecules on metal surfaces.

Before we proceed to a more detailed discussion of the binding of adsorbed molecules, a few remarks concerning the electronic structure of oxide surfaces are appropriate.

Early on, Hüfner and co-workers investigated the electronic structure of transition metal bulk samples and a great deal has been learned.[61,62] There have also been attempts to investigate the surfaces of these materials with respect to electronic structure. Qualitatively, it was expected that, due to the high ionicity of some compounds, there are pronounced surface effects. Photoelectron

spectroscopy has been used to experimentally verify these expectations through the detection of chemically shifted core levels. However, the shifts are not large enough to be detectable due to the relatively complex satellite structure accompanying metal core ionization.[62] Eventually, this was also rationalized *via* more sophisticated quantitative calculations which showed that there are several compensating contributions rendering the surface fields only slightly different from the bulk. Applying techniques allowing for higher energy resolution have then clearly demonstrated surface effects. In the Merz group[63] and our laboratory[64] electron energy loss spectroscopy (EELS) in the regime of electronic excitations has been used to identify excitations in the surface layer. Fig. 5 shows a set of spectra taken on Ni(100) surfaces. The lowest trace has been taken on a clean single crystal. The broad features peaking at 4–5 eV correspond to charge-transfer excitations crossing the band gap of the insulating NiO bulk. In the gap there are narrow features due to excitations within the d-electron state manifold of the open shell Ni^{2+} ions. As the excitation energy within this manifold increases the number of states increases, so that near the charge-transfer band those states overlap and lead to the monotonous increase of intensity in this energy region. Most of the optically allowed transitions have been spectroscopically observed by transmission spectroscopy of bulk samples.[65–67] Fromme and Kisker have recently performed spin-polarized EELS measurements, which allow an assignment of the spin character of all states *via* the control of spin-polarization in the scattering conditions.[68,69] The assignment and a spin-polarization measurement have been superimposed on the spectra. The important point here is

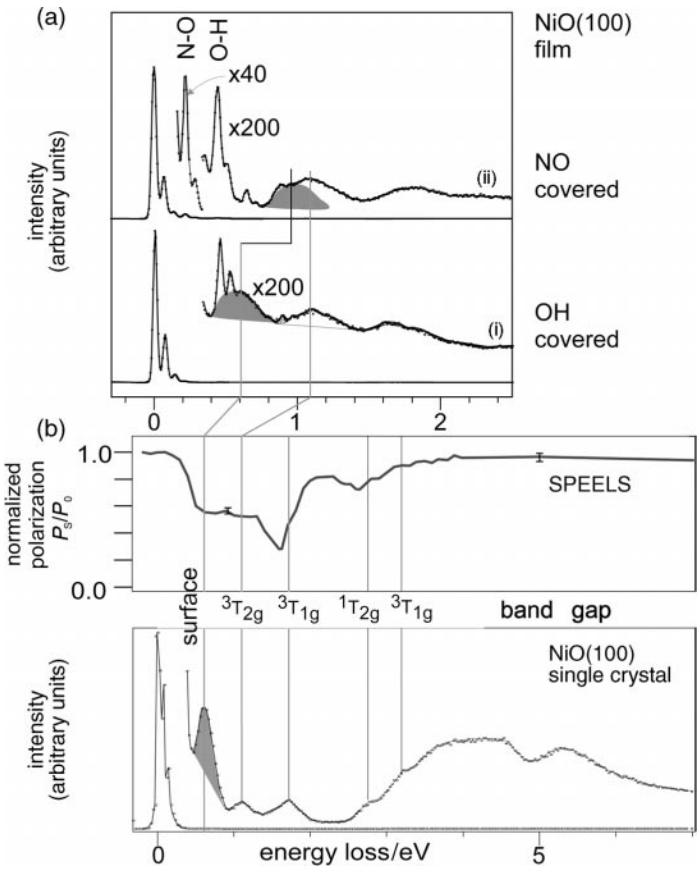

Fig. 5 Electron energy loss spectra of NiO(100) surfaces. (a) Adsorbate covered NiO(100) films, (i) defects OH saturated, before NO adsorption, (ii) after adsorption of NO. (b) Clean NiO(100) surfaces, UHV-cleaved single crystal. The assignment of the features according to theory is given and supported by spin-polarized measurements (adapted from ref. 68 and 69).

that there are additional spectroscopic features, most pronounced at 0.6 eV excitation energy which are not due to excitations in the bulk but rather in the surface layer. This can be experimentally demonstrated by an adsorption study.[64] Those excitations localized in the surface should be most strongly affected by adsorbed species. The experiment has been performed on a thin film sample because the surface has to be cooled to adsorb an appreciable amount of NO in this case. It is very obvious that the peak at 0.6 eV is influenced. In fact, it is shifted towards the position of a feature originating from an excitation in the bulk. In passing we note that the NiO(100) film has been treated with water before the experiments had been performed, in order to saturate the defects with hydroxy groups *via* dissociative adsorption of water. The vibrational losses caused by the hydroxys are clearly visible before NO adsorption took place. NO adsorption then induces yet a further vibrational loss at lower loss energy. What is the nature of the surface excitation and why is it different from the bulk excitation? Staemmler and his group have performed *ab initio* cluster calculations,[64,70] the result of which can be summarized as follows: Due to the localization of the Ni-d-electrons it is sufficient to consider a single Ni^{2+} ion within its octahedral coordination sphere if we consider the situation encountered in the bulk (see Fig. 6). The ground state is a ^3E state with two unpaired d-electrons in the e_g orbitals of the ligand field split set of d-orbitals. The first excited state results from an excitation from the completely filled t_{2g} subset into the partly filled e_g subset giving rise to an excitation located near 1 eV. There are many more higher excited states, some of which are assigned according to the work of Fromme *et al.*[68,69] In the surface, however, one of the coordinated oxygen ions is missing and the symmetry of the local Ni^{2+} site is reduced to C_{4v}. Consequently, the degenerate e_g subset is split. The t_{2g} subset is also

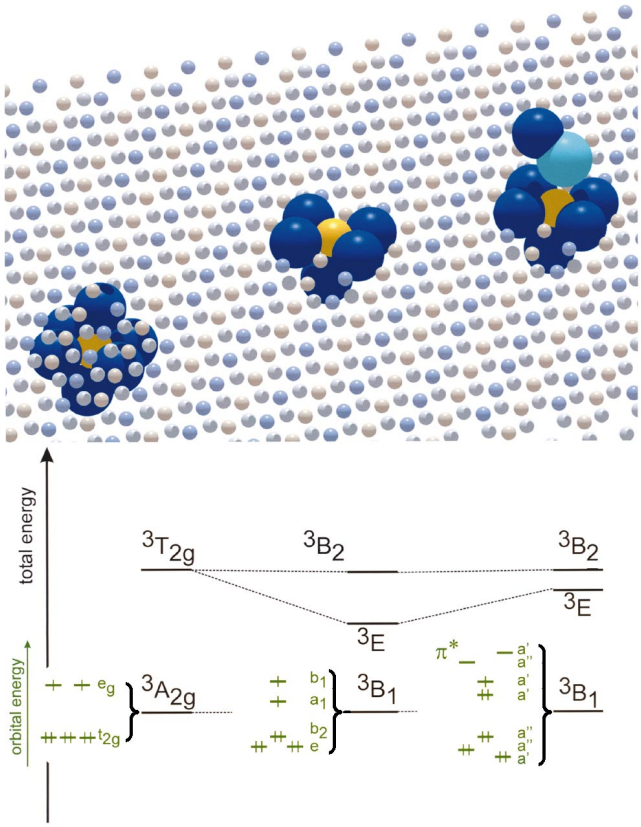

Fig. 6 Correlation of structural data with electronically excited states on NiO(100). Upper panel: (left) coordination of a Ni ion in the bulk, (middle) coordination of a Ni ion in the clean (100) surface as well as (right) in the case of adsorbed NO. Lower panel: orbital diagram and total energies from cluster calculations.[64,70]

split, but this effect is not so important. The d-orbital of the former e_g subset pointing along the Ni–O axis has lost part of its destabilizing interaction and, consequently, its energy decreases. The calculation shows that still both orbitals in the former e_g subset are singly occupied after reduction of symmetry. Therefore, the first excited state in a Ni^{2+} surface ion is at lower energy than in the bulk, as also revealed by the experiment. If an NO molecule is now coordinated to the Ni^{2+} surface ion, the energetic position of the orbital is raised again (similar to the presence of the sixth oxygen ion), effectively moving the excitation energy back close to the bulk position. It is clear from these results that the surface effect on the excitation energies is of the order of 0.4 eV, and thus the above mentioned lack of evidence from other techniques can be rationalized.

So far we have discussed the localized metal-ion states. Are there also surface modifications onto the charge-transfer states? The answer is yes! Unfortunately, NiO is not a good example to support this experimentally. The electronic excitations of the $Cr_2O_3(0001)$ surface, on the other hand, show the effect very clearly.[71–74] Fig. 7 shows the EELS spectrum[72–74] of this surface at low temperature. Again, a thin film has been used. The sharp features in the band gap are excitations within the manifold of d-orbitals. A detailed discussion[74] has shown that the excitations are characteristic of surface Cr ions with three d-electrons. However, the Cr ions do not carry a net charge of 3+ as expected (and found for the bulk Cr ions) but rather of 2+ charge due to strong hybridization with the neighboring oxygen atoms. When we now perform EELS measurements after adsorption of CO_2, not only the d-excitations are influenced but also the very intense feature near 3.8 eV. Again, on the basis of cluster calculations performed in the Staemmler group,[71] it has been possible to assign this intense feature to a surface charge-transfer excitation at the band gap, which is shifted to lower energy as compared with the corresponding excitation in the bulk (see Fig. 7). The decrease in energy is reasonable because the Cr d-orbitals have been lowered, the more open surface structure (see Fig. 3), and the coordination of the Cr ions to only three oxygen ions allows for better charge separation than in the bulk. In NiO the effect is less pronounced because the surface Ni ions are still five-fold coordinated.

The analysis of the electronic structure of $Cr_2O_3(0001)$, as discussed so far, has been performed at 90 K. We note that upon increasing the temperature, the structure of the surface changes,[74] and we have speculated that these changes are connected with changes in the magnetic structure of the surface. Oxide surface magnetism is a field that needs to be explored in the future.

At this point we return to the question raised above, on the binding and interaction of molecules with oxide surfaces. Molecules bind to oxides *via* a bonding mechanism considerably different from metal surfaces. A CO molecule, for example, binds to metals *via* chemical bonds of varying strength involving charge exchanges.[75] Fig. 8 illustrates the bonding of CO to a Ni-metal atom *via* the so-called σ-donation/π-back-donation mechanism schematically, and on the basis of a one electron orbital diagram.

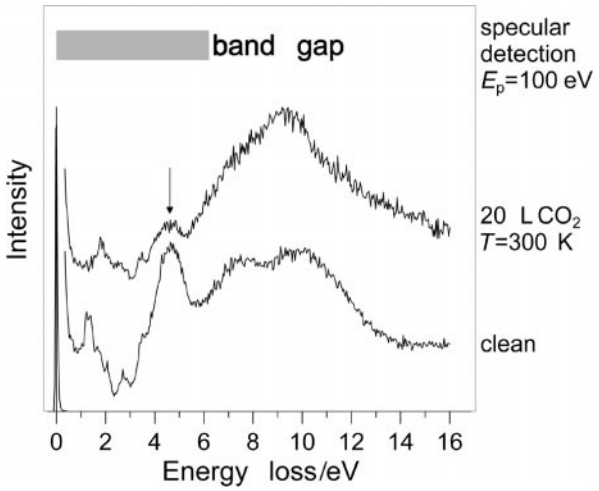

Fig. 7 EELS spectra of the clean and adsorbate covered $Cr_2O_3(0001)$ surface.[72–74]

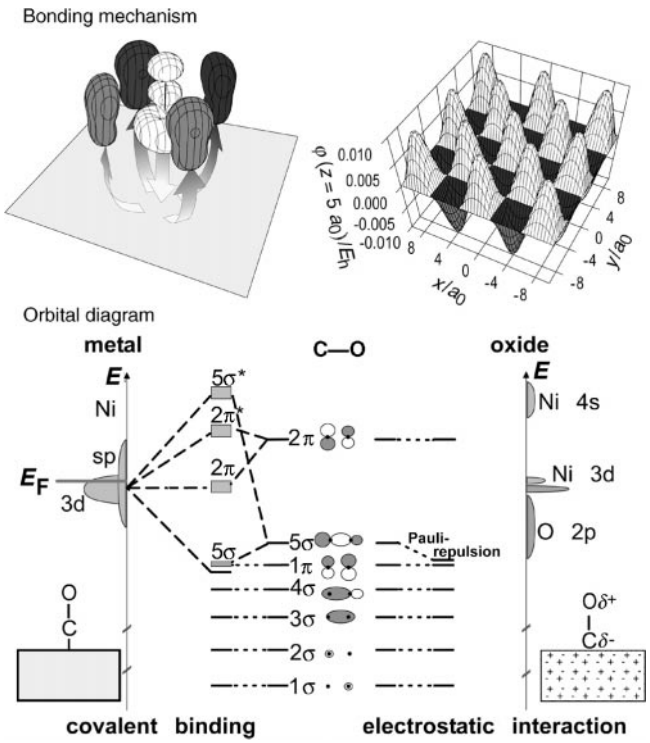

Fig. 8 Orbital diagram for the bonding of CO to Ni-metal (left) and to Ni-oxide (right).

The σ- and π-interactions lead to a relative shift of those σ- and π-orbitals involved in the bond with respect to those orbitals not involved. The diagram reflects this *via* the correlation lines. This may be contrasted by the electrostatically dominated interaction between a CO molecule and a Ni ion in nickel oxide.[70,76] There is a noticeable σ-repulsion between the CO carbon lone pair and the oxide leading to a similar shift of the CO 5σ-orbital as in the case of the metal atom. However, there is no or little π-back-donation so that the CO π-orbitals are not modified.[11,77] Conceptually, the situation is transparent and one would expect that a detailed calculation reveals the differences quantitatively. However, as it turns out the description by *ab initio* calculations is very much involved and today a full account cannot be given.[78] Theoretically (Table 1)[70,78–89] the prediction is that CO as well as NO bind very weakly to NiO.[78] The predicted binding energy of CO is of the order of 0.1 eV and it is expected to be similar to CO binding to MgO(100), *i.e.* the influence of the Ni d-electrons should be negligible.[78]

To shed light on this problem it was necessary to perform thermal desorption measurements on cleaved single crystal surfaces, being the surfaces with the least number of defects.[90] In Figs. 9 and 10 TDS data for CO and NO on vacuum-cleaved NiO(100) are compared with data for thin NiO(100) films grown by oxidation of Ni(100). At temperatures of 30 and 56 K multilayer desorption for CO and NO, respectively, shows up. The pronounced features at higher temperatures correspond to desorption of the respective adsorbate at (sub)monolayer coverage. In the case of the CO adsorbate at 34 K desorption of the second layer is found and the states at 45 and 145 K for CO and NO, respectively, are due to adsorption on defects as concluded from data obtained from ion bombarded surfaces (not shown here). It is obvious that for both adsorbates the thin film data and the data of the cleaved samples agree well, in particular for NiO(100) the thin film data are comparable to those from the more perfect surfaces of the cleaved samples. The higher defect density of the thin film surfaces leads to small, but clearly visible additional peaks in the TDS data which show up as shoulders near to the main peak, for example in the NO spectra. Nevertheless, the general shapes of the thin film spectra of both adsorbates are very similar to those of the cleaved samples.

Table 1 Table of literature data for adsorption of CO and NO on NiO(100) and MgO(100)[a]

Author	System	Method	Adsorption energy eV
Pacchioni and Bagus[79]	CO/NiO(100)	*Ab initio* cluster calculation	0.24
Klüner and Freund[80]	NO/NiO(100)	*Ab initio* cluster calculation, BSSE correction	≈0
Pöhlchen and Staemmler[70]	CO/NiO(100)	*Ab initio* cluster calculation, BSSE correction	0.03 to 0.1
Cappus *et al.*[81]	CO/NiO(100)/Ni(100)	TDS, Redhead	0.32
Vesecky *et al.*[82]	CO/NiO(100)/Ni(100)	IRS, Clausius–Clapeyron	0.45
Staemmler[83]	NO/NiO(100)	*Ab initio* cluster calculation, BSSE correction	0.1
Pöhlchen[84]	NO/NiO(100)	*Ab initio* cluster calculation, BSSE correction	<0.23
Kuhlenbeck *et al.*[85]	NO/NiO(100)/Ni(100) and NO/NiO(100)	TDS, Redhead	0.52
Nygren and Pettersson[78]	CO/MgO(100)	*Ab initio* cluster calculation, BSSE correction	0.08
Chen *et al.*[86]	CO/MgO(100)	DFT	0.28
Neyman *et al.*[87]	CO/MgO(100)	DFT, BSSE correction	0.11
He *et al.*[88]	CO/MgO(100)/Mo(100)	IRS, Clausius–Clapeyron, TDS, Redhead	0.43 0.46
Furuyama *et al.*[89]	CO/MgO powder	IRS, Clausius–Clapeyron	0.15 to 0.17

[a] BSSE, basis set superposition error; TDS, thermal desorption spectroscopy; DFT, density functional theory; IRS, infrared spectroscopy; Clausius–Clapeyron, evaluation of pressure and temperature dependent IR intensities with the Clausius–Clapeyron equation; Redhead, evaluation of TDS data with the Redhead equation.[179]

For CO the shift of the peak maximum with increasing coverage indicates that at higher coverage repulsive lateral interaction comes into play which may lead to occupation of energetically less favorable sites. This is not the case for the NO adsorbate which may be attributed to smaller lateral interactions and to the higher adsorption energy which makes adsorption more site specific, and thus may inhibit compression of the layer involving site changes.

TDS data for NO and CO on vacuum-cleaved MgO(100), for comparison, are plotted in Figs. 11 and 12. Multilayer desorption is found at 29 and 56 K for CO and NO, respectively. The small features around 45 and 100 K are likely due to defect adsorption since they saturate at rather low coverage. Desorption from layers with small coverage is found at 57 and 84 K for CO and NO, respectively. The data for CO and NO on NiO(100) have been evaluated using the leading edge method as well as a complete analysis. Details of the procedures may be found in ref. 91 and 92. Both methods determine the heat of adsorption as a function of the coverage of molecules already on the surface. The results of the evaluation are shown in Figs. 13 and 14. Both graphs exhibit a trend which is generally to be expected for laterally interacting adsorbate layers: the adsorption energy decreases with increasing coverage. At coverages near to 1 monolayer the energies converge towards the multilayer values (0.09 and 0.18 eV for CO and NO, respectively[93]). At low coverage the lateral interactions are most likely small so that the corresponding adsorption energies may be compared with theoretical results since in the calculations lateral interactions have not been considered. As indicated in Figs. 13 and 14, the low coverage adsorption energies are 0.30 and 0.57 eV for CO and NO, respectively.

The low coverage adsorption energies for CO and NO on NiO(100) and MgO(100) are compiled in Table 2. According to theory the interaction of the adsorbates with MgO(100) and NiO(100) are expected to be similar since the bonding should be mainly electrostatic in nature[78] (the electric fields at the surfaces of NiO(100) and MgO(100) are similar). However, according to Table 2 the bonding energies are considerably different, with the higher values being obtained for NiO(100). Covalent interactions involving the Ni 3d-electrons may play a role for the adsorbate–substrate interaction which does not show up in the calculations published so far.

As far as it concerns the basis set superposition error (BSSE) corrected calculations listed in Table 1 which are expected to yield qualitatively better results as compared to the non-corrected

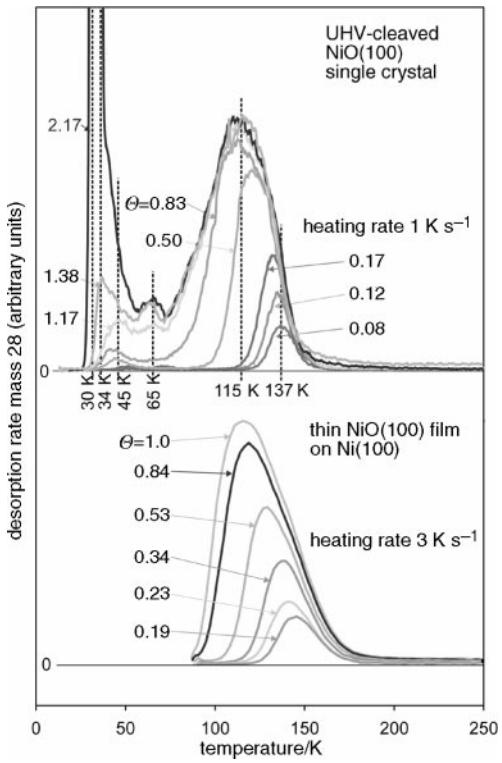

Fig. 9 Thermal desorption spectra of CO on NiO(100) cleaved in vacuum (upper part) and CO on a thin NiO(100) film grown by oxidation of Ni(100) (lower part). The mass spectrometer was set to mass 28 (CO). CO doses are given relative to the dose needed to prepare a monolayer.

calculations, it appears that the theoretical results for adsorption on MgO(100) are in general in line with our experimental results, whereas a similarly favorable comparison can not be made for NiO(100). It appears necessary to re-investigate the role of the Ni 3d-electrons in future theoretical studies.

The adsorption of CO on MgO has been thoroughly investigated by Heidberg and his group using IR-spectroscopy[94] and by Weiss and co-workers using helium scattering spectroscopy.[95] They have clearly demonstrated that CO develops ordered phases on the cleavage planes and that order and spectroscopic properties depend on the quality of the prepared surfaces. From their experiments the influence of the presence of surface defects on adsorption properties is very obvious but a quantitative evaluation based on the number and the nature of the defects has not been reported.

The quantitative evaluation of defects is a well defined but hard to tackle problem for future studies that has to be taken on by our research community. Water adsorption is an example that lends itself to a study of the influence of defects, because at lower coverage the (100) cleavage planes of MgO and NiO do not dissociate water, while the presence of defects does induce water

Table 2 Compilation of low-coverage bonding energies for NO and CO on NiO(100) and MgO(100) obtained in this work

	NiO(100)	MgO(100)
CO	0.30 eV	0.14 eV
NO	0.57 eV	0.22 eV

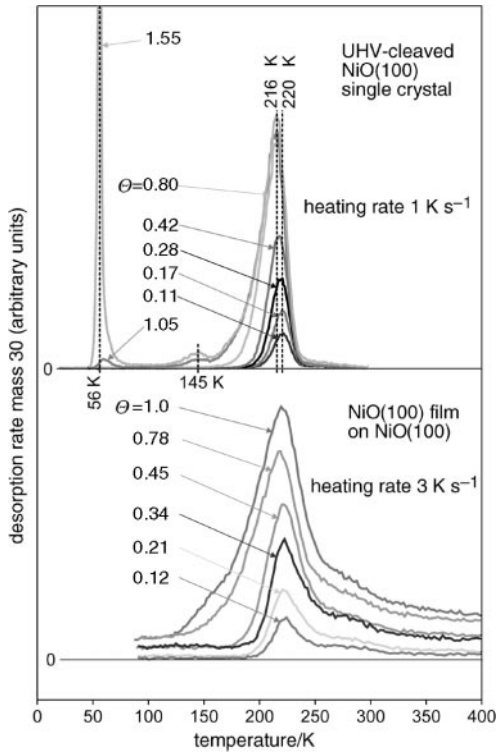

Fig. 10 Thermal desorption spectra of NO on NiO(100) cleaved in vacuum (upper part) and NO on a thin NiO(100) film grown by oxidation of Ni(100) (lower part). The mass spectrometer was set to mass 30 (NO). NO doses are given relative to the dose needed to prepare a monolayer.

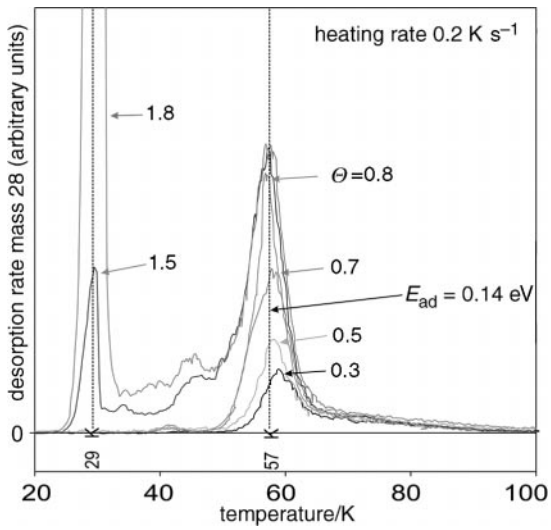

Fig. 11 Thermal desorption spectra of CO on MgO(100) cleaved in UHV. The mass spectrometer was set to mass 28 (CO). CO doses are given relative to the dose needed for the preparation of a monolayer.

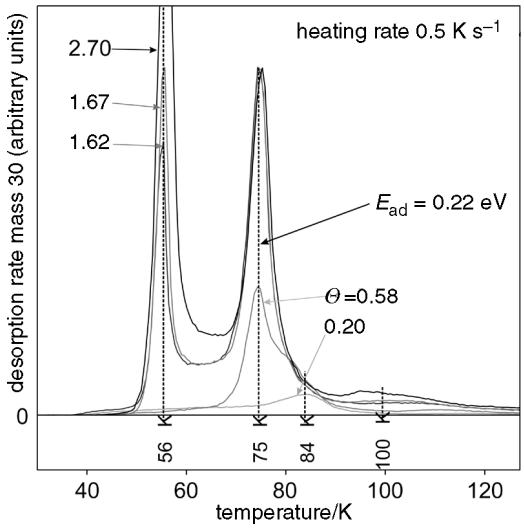

Fig. 12 Thermal desorption spectra of NO on MgO(100) cleaved in UHV. The mass spectrometer was set to mass 30 (NO). NO doses are given relative to the dose needed for the preparation of a monolayer.

dissociation. This can be seen in TDS spectra of H_2O from (100) rock-salt type surfaces. Fig. 15 shows results for H_2O desorption from MgO(100) and NiO(100).[96] The most pronounced features in the spectra are due to condensed water layers at lowest desorption temperature and the conversion of a compact layer (with c(4 × 2) periodicity in the case of MgO) to the monolayer which desorbs at 225 K (240 K for MgO(100).[97,98] The difference in desorption temperature between

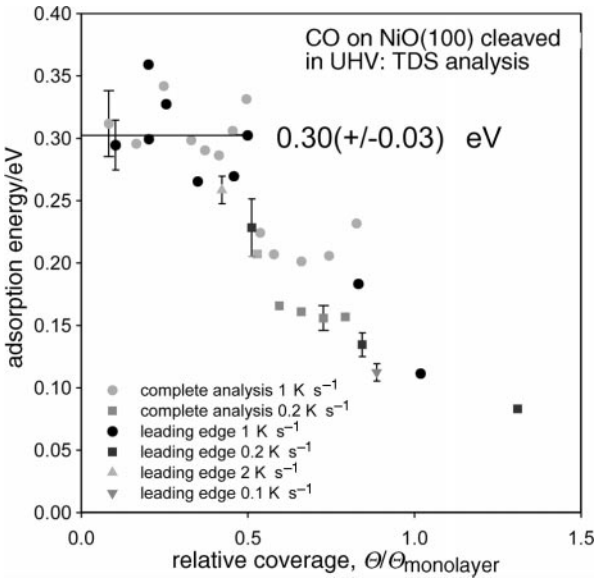

Fig. 13 Adsorption energy of CO on NiO(100) cleaved in vacuum as a function of coverage. The data have been determined from TDS spectra like those shown in Fig. 9 (upper part) using the leading edge method and complete analysis. TDS data taken with heating rates of 0.1, 0.2, 1 and 2 K s^{-1} have been used.

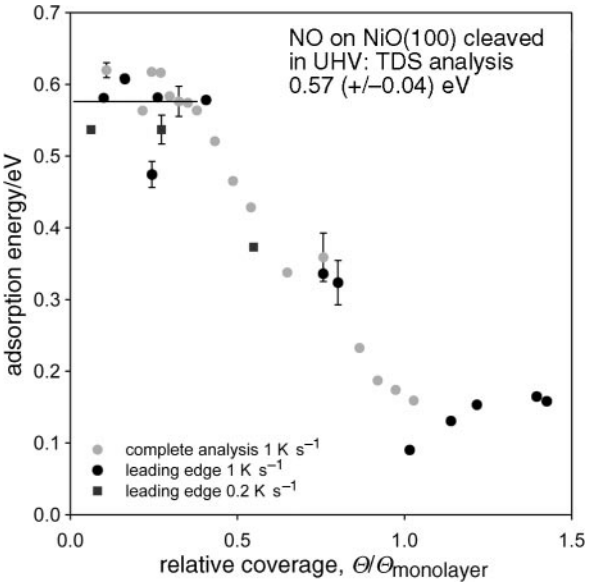

Fig. 14 Adsorption energy of NO on NiO(100) cleaved in vacuum as a function of coverage. The data have been determined from TDS spectra like those shown in Fig. 10 (upper part) using the leading edge method and complete analysis. TDS data taken with heating rates of 0.2 and 1 K s^{-1} have been used.

MgO(100) and NiO(100) seems to be characteristic for the H_2O substrate interaction. Most of that information is lost when we create defects *via* sputtering. Thermal desorption is now observed up to relatively high temperatures and the features are broad. Which kind of defects and how many have been created is not yet known. A combination of various techniques to characterize the defects by probe molecule adsorption together with infrared spectroscopy, EPR and electron spectroscopies may in the future lead to a deeper understanding.

Dissociative adsorption of water on oxide surfaces can also be used in a preparative way, namely to chemically modify the surface by hydroxylation. We have used this technique for a thin alumina film to study the influence of the presence of hydroxy groups on the nucleation and growth of metallic aggregates as will be discussed later.[99] At this point we show in Fig. 16 the result of such a hydroxylation as measured with vibrational spectroscopies, such as high resolution electron energy loss spectroscopy (HREELS) and FTIR.[100] In the case of the thin alumina film on NiAl(110) it was impossible to hydroxylate the oxide just by water dissociation, while on a similar film on NiAl(100)[101] formation of OH from dissociative H_2O adsorption occurs. The clean oxide film surface was exposed to metallic aluminium and then the aluminium was hydrolyzed *via* water adsorption to form a hydroxy overlayer.[99,100] In Fig. 16 at the bottom an HREELS spectrum showing the hydroxy vibration at 465 meV (3750 cm^{-1}) is plotted atop a corresponding spectrum of the clean film. The peaks below 120 meV are due to the alumina phonons,[102] which are broadened through hydroxylation influencing surface order. The observed hydroxy loss coincides very nicely with the FTIR absorption observed for the same system. In this case more water was adsorbed so that a broad band from water clusters is seen also. The sharp extra band at 3705 cm^{-1} is due to free OH groups at the surface of these water clusters,[103] as they are known from the surface of ice. In fact, if a thick ice film is grown on the alumina film this particular vibration is observed (see Fig. 16). In comparison with literature data[104] it is now possible to assign the hydroxy loss on the alumina surface. According to a review article by Knözinger[104] an OH-vibration at 3750 cm^{-1} is characteristic of hydroxys bridging aluminium ions both in octahedral, or one in an octahedral and one in a tetrahedral site. We mention that on alumina films grown on a different NiAl substrate[101] other types of OH species may be formed as was shown by Hemminger's group. Therefore, it is conceivable that the influence of the nature of

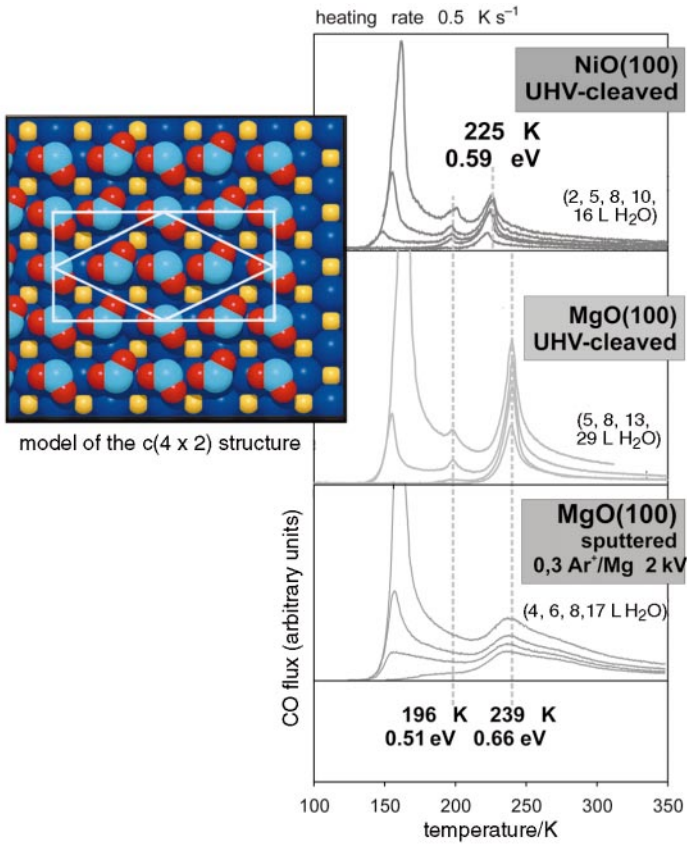

Fig. 15 Thermal desorption spectra of H_2O on UHV-cleaved MgO(100) and NiO(100). A schematic representation of the c (4 × 2) structure is included (reproduced from Heidberg, Redlich and Wetter, *Ber. Bunsenges. Phys. Chem.*, 1995, **99**, 1333). For comparison a thermal desorption spectrum from MgO(100) after creation of defects *via* sputtering is shown.

the hydroxy species modifying the surface on the interaction with additional adsorbates, *i.e.* metal deposits, could be investigated.

Before we move on to discuss the properties of metals on oxides we would like to briefly discuss the adsorption of CO_2 on oxides as an example of a molecular adsorbate system with more degrees of freedom.

TDS spectra indicate[105,106] that there are more weakly and less weakly bound CO_2 species on a Cr_2O_3(0001) surface. We have studied the nature of those species by various techniques including infrared spectroscopy. Fig. 17 shows several sets of IR spectra. The pair of sharp bands around 2300 cm^{-1} can easily be assigned to the more weakly bound CO_2 with only a slightly distorted structure as compared with the gas phase species. By a combination of isotopically labeling the adsorbed CO_2 (shift of frequencies) as well as the oxide layer (no shift of CO_2 bands) we have demonstrated that the single band centered around 1400 cm^{-1} is due to the presence of a carboxylate species, *i.e.* a bent anionic CO_2 species, and not, as perhaps expected, to a carbonate.[72] The bands between 1610 and 1700 cm^{-1} are missing because of the applicability of surface selection rules in thin film systems. This means, all non-totally symmetric bands are suppressed in intensity. A quick comparison with CO_2 adsorption on chromia microcrystalline material as shown in Fig. 17 indicates the presence of the bands between 1610 and 1700 cm^{-1} as expected for adsorption on a bulk dielectric material. It is remarkable how similar the thin film data are in comparison with the microcrystalline material. This has been discussed in detail by Zecchina's group.[107] Also, the

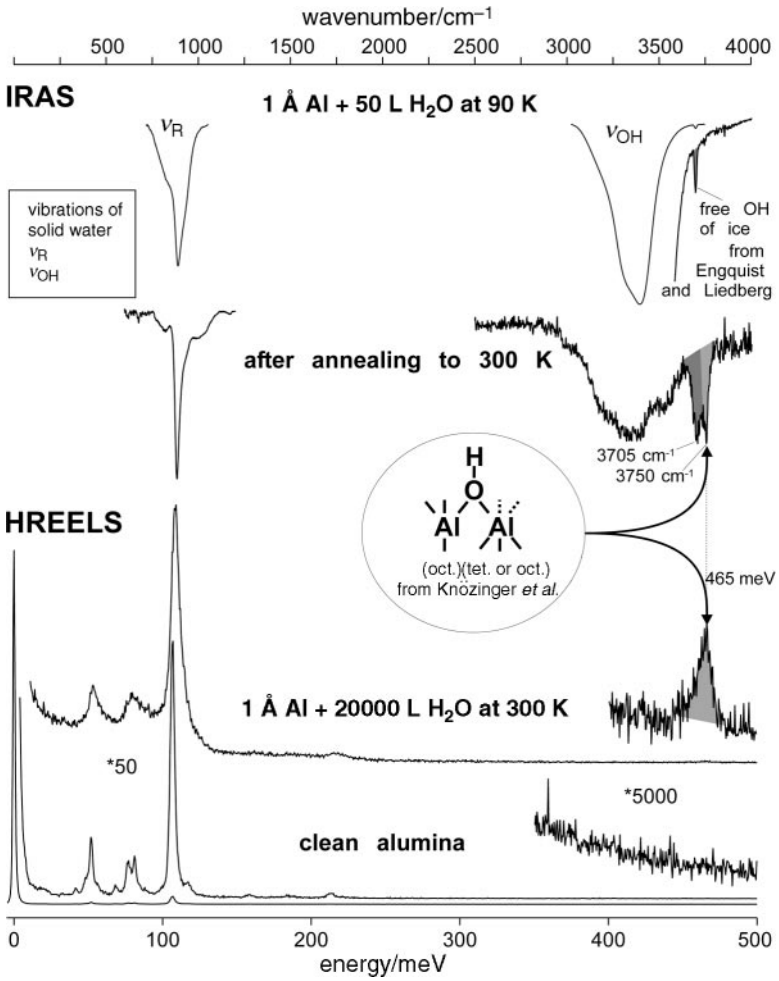

Fig. 16 Fourier transform IR spectra (IRAS) and electron energy loss spectra (HREELS) of a clean and $OH(+H_2O)$-covered alumina film.

response of the two systems with respect to preadsorption of oxygen is very similar. In fact, as shown in Fig. 17, CO_2 adsorption in the form of the less weakly bound CO_2^- is fully suppressed on the thin film system and very strongly attenuated for the microcrystalline system. This indicates that CO_2 occupies the chromium sites, because we know that oxygen from the gas phase adsorbs on the chromium ions. As we remarked above, ELS[73] and XPS[108] spectra of the $Cr_2O_3(0001)$ surface have been used to deduce that the Cr-ions in the surface are in a low oxidation state, *i.e.* Cr^{2+} as opposed to chromium ions in the near surface and bulk regions. It is therefore not surprising that such a surface provides electrons to adsorbed molecules, leading to electron transfer as, for example, documented by the formation of O_2^- and CO_2^-. The low valence state of the Cr surface ions also has consequences in other reactions, such as the polymerization of ethene which has been studied on $Cr_2O_3(0001)$,[109] and in connection with other, more realistic model studies.[110]

A field that has not been investigated in any detail as far as well characterized single crystal oxide surfaces are concerned is connected with photoinduced chemical reactions on larger molecules. Photoinduced desorption of CO and NO from oxides has been studied extensively[111–114] but the reactivity of larger molecules has not. Yates and his group have reported such studies on

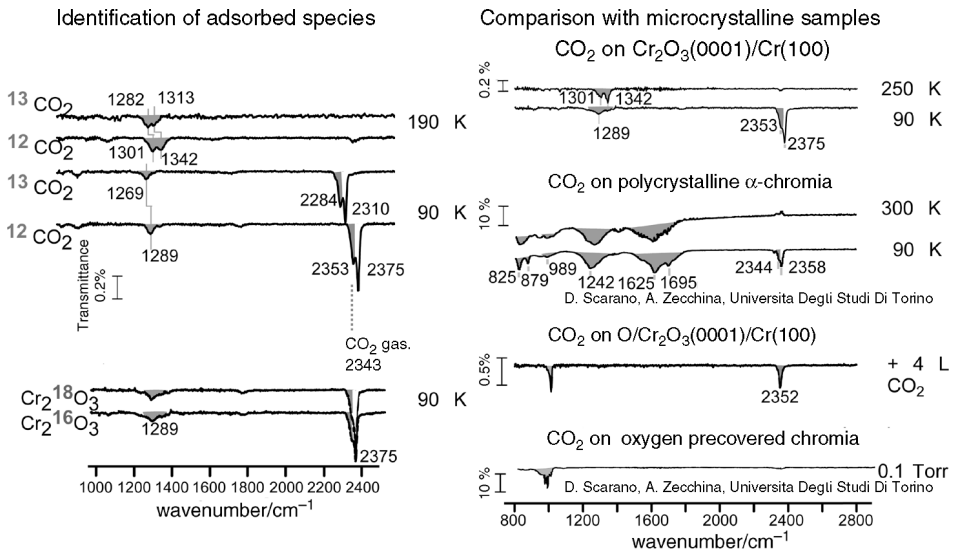

Fig. 17 IRAS spectra of CO_2 adsorbed on Cr_2O_3(0001) surfaces and on polycrystalline chromia. Left panel: IRAS spectra at different surface temperatures and with isotopically labelled CO_2 as well as Cr_2O_3. Right panel: adsorption of CO_2 after pre-adsorption of oxygen.

powder samples, *i.e.* Rh complexes deposited on Al_2O_3 powder and very interesting results concerning C–H bond activation have been reported.[115] We refer to the literature for details,[115] and note that this should be considered as a new promising area in connection with single crystalline systems.

Metals on oxides

So far, we have considered the clean oxide surface and its reactivity. In the following we will modify the oxide surface by deposition of metal onto the surface. This represents a route towards the preparation and characterization of more complex model systems in heterogeneous catalysis in order to bridge the so-called materials gap.

Over past years several strategies have been followed along this route. Very early on small metal particles have been put onto oxide bulk single crystal surfaces, particularly MgO, and characterized by transmission electron microscopy (TEM). Poppa has been the pioneer in this field,[18] and the very important contributions to the field have been recently reviewed by Henry, who himself was involved in the early TEM measurements.[14] While these efforts where mainly aimed at preparing small well defined particles, another strategy has been followed by Møller and his group[116–119] as well as Madey and co-workers[19] by trying to prepare thin metal films on bulk oxide single crystals, such as TiO_2(110) surfaces. As mentioned above the advent of scanning tunneling microscopy has had a substantial influence on the understanding of the structure of clean oxide surfaces. Several groups[120–122] have started to investigate metal deposition on TiO_2 surfaces. Interesting initial results concerning metal particle migration, and oxide migration onto the metal particles (the so-called SMSI effect) have been obtained.[121,122] Particularly well suited for the application of scanning tunneling microscopy are metal particles deposited onto thin film oxide surfaces.[8,10,11,14] Goodman's group, for example, made major contributions to this field early on.[10] In Fig. 18 we show the result of a STM study from our laboratory. The left panel shows the clean alumina surface as imaged by a scanning tunneling microscope.[123] The surface is well ordered and there are several kinds of defects on the surface: Firstly, the reflection domain boundaries between the two growth domains of Al_2O_3(0001) on the NiAl(110) surface, the substrate on which the film is grown *via* a well established oxidation recipe.[102] Secondly, there are anti-phase domain boundaries within the reflection domains, and in addition, there are point defects which are not resolved in the images. The image does not change dramatically after

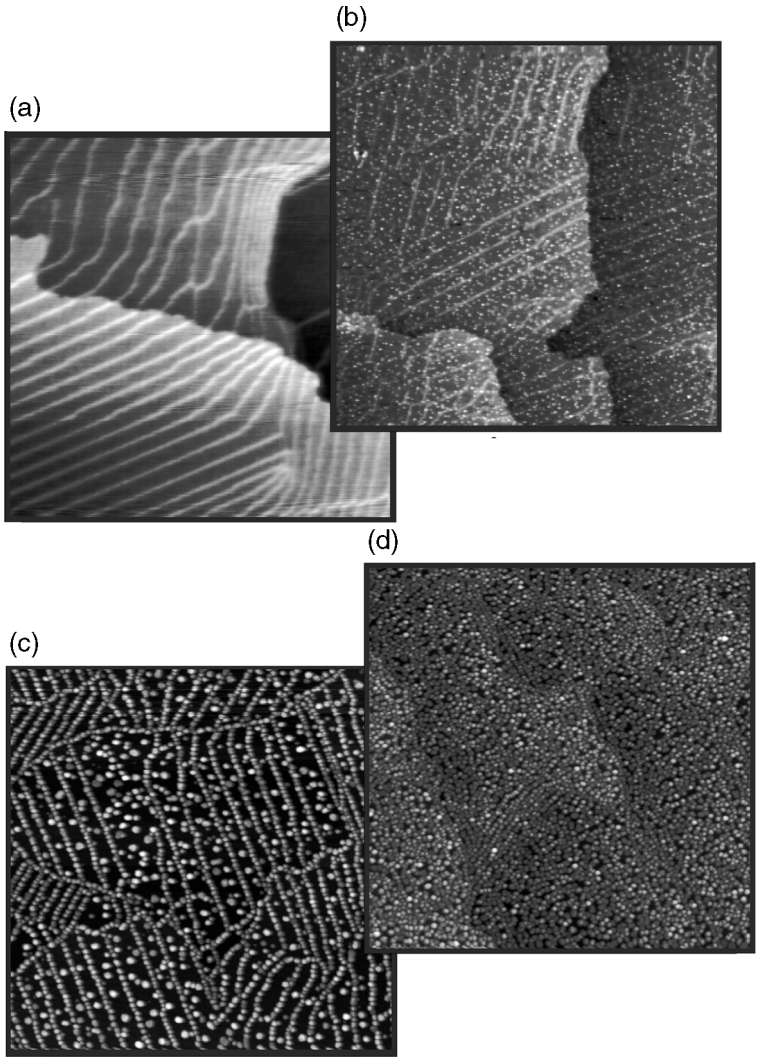

Fig. 18 Scanning tunneling images (3000 × 3000 Å^2, Al_2O_3/NiAl(110), $u_{tip} = 8$ V, I = 0.8 nA). (a) Clean alumina film, (b) after deposition of 0.1 Å of Rh at 90 K, (c) after deposition of 2 Å of Rh at 300 K, and (d) after deposition of 2 Å of Rh at 300 K on hydroxylated substrate onto the pre-hydroxylated alumina film.

hydroxylating the film, a procedure we had mentioned above.[99] The additional panels show STM images of rhodium deposits on the clean surface at low temperature, and at room temperature,[15,124] as well as an image after deposition of Rh at room temperature on a hydroxylated substrate.[125] Please note, that the amount deposited onto the hydroxylated surface is equivalent to the amount deposited onto the clean alumina surface at room temperature. Upon deposition of Rh from the metal vapor onto the clean surface at low temperature small particles nucleate on the point defects of the substrate and a narrow distribution of sizes of particles is formed. If the deposition of Rh is carried out at room temperature the mobility of Rh atoms is considerably higher compared with low temperature so that nucleation at the pronounced line defects of the substrate becomes dominant. Consequently, all the material nucleates on the reflection domain and anti-phase domain boundaries. The particles have a relatively uniform size given by the amount of deposited material. If the same amount of material is deposited onto a hydroxylated surface the particles are considerably smaller and distributed across the entire surface showing

that hydroxylation leads to higher metal dispersion.[15,99] The thermal behavior of the deposits is important with respect to studies of chemical reactivity because the ensemble of particles may undergo morphological changes adopting their equilibrium shape which could be different with and without the presence of a reactive gas phase. In the present case detailed studies have been undertaken on the particles deposited onto the clean substrate and less detailed studies for the deposit on the hydroxylated surface. As a result of these studies it is known that the morphology of the ensemble is not altered within a temperature window from 90 to approximately 450 K. The window is extended to even higher temperatures on the hydroxylated substrate. Above the upper temperature limit the particles tend to agglomerate and also start to diffuse through the film into the metal substrate underneath.[15]

Studying this agglomeration process is an interesting subject in itself and research in this direction is only starting.[15] A more basic aspect, of course, would be a study of metal atom diffusion on oxide substrates. The obvious method to perform such a study is the STM.[126] However, in contrast to diffusion studies on metal surfaces, similar studies on oxide surfaces have not been reported. On the other hand, field ion microscopy studies on metal atom diffusion on oxide films are under way and a first estimate of activation energies for diffusion has been reported.[127] It is obvious that the area of diffusion studies will considerably profit from atomic resolution, once it is obtained routinely for deposited aggregates on oxide surfaces. While for TiO_2 and very few other oxide substrates atomic resolution may be obtained routinely, there are very few studies on deposited metal particles where atomic resolution has been reported.[128] The first report for an atomically resolved image of a Pd metal cluster on MoS_2 was reported by Henry and his group.[128] A joint effort between Besenbacher and our group[129] has led to atomically resolved images of Pd aggregates deposited on a thin alumina film. Fig. 19 shows such an image of an aggregate of about 80 Å in width. The particle is obviously crystalline and exposes on its top facet, the (111) Pd surface. Also, the (111) facets on the side, typical for a cuboctahedral particle, can be discerned. The small (100) facets predicted *via* equilibrium shape considerations on the basis of the Wulff-construction could not be atomically resolved. If we, however, apply the concept of the Wulff-construction, we may deduce the metal surface interaction energy.[129] The basic equation is

$$W_{\mathrm{adh}} = \gamma_{\mathrm{oxide}} + \gamma_{\mathrm{metal}} - \gamma_{\mathrm{interface}} \quad (1)$$

Provided the surface energies (γ_{metal}) of the various crystallographic planes of the metal are known,[130] a relative work of adhesion (W_{adh}) may be defined.[129] We find 2.9 ± 0.2 J m^{-2} which is still rather different with respect to recent calculations by Jennison *et al.*[131] where metal adsorption energies (1.05 J m^{-2}) have been calculated on a defect free thin alumina film. It is not unlikely that this discrepancy is connected with the rather complicated nucleation and growth behavior of the aggregates involving defects in the substrate.

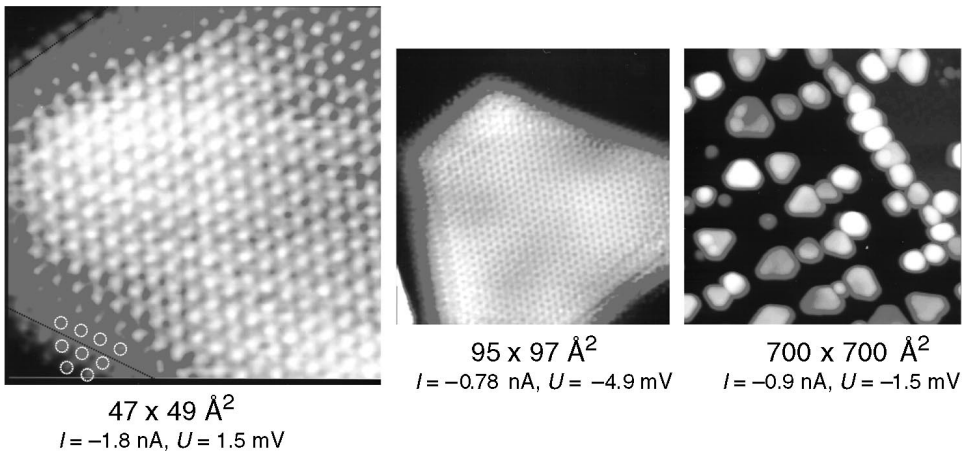

Fig. 19 Scanning tunneling images at atomic resolution of Pd aggregates grown on an alumina film.[129]

While STM reveals the surface structure of deposited particles, their internal structure, in particular as a function of size, is not easily accessible through STM. In this connection TEM studies on the same model systems can be of help.[132] Fig. 20 shows a schematic drawing of a sample. After growing the film and deposition of the particles, the sample is ion-milled from the back so that a small hole is finally formed. In this way, a wedge is obtained which is thin enough for the imaging process. A positive side effect of this procedure is the fact that also the unsupported film next to the edge can be studied.[133] This opens the opportunity to judge whether the metal substrate has any structural effect on the deposits. On the basis of numerous high resolution TEM images and a subsequent analysis of the Moiré periodicities, it has been possible to calculate the lattice constants as a function of particle size.[132] The corresponding plot is depicted in Fig. 21 and indeed proves that the atomic distances continuously decrease to 90% of the bulk value at a cluster size of 10 Å. On the other hand, the lattice constant approaches the Pt bulk value already at a diameter of 30 Å. This effect has also been detected for Ta and Pd clusters on the thin alumina film, but it seems to be less pronounced in these cases.[134–136]

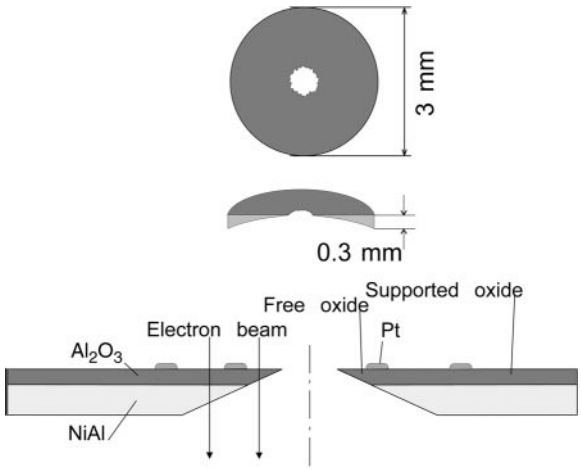

Fig. 20 Schematic drawing of a sample prepared for transmission electron microscopy (sample milling technique).

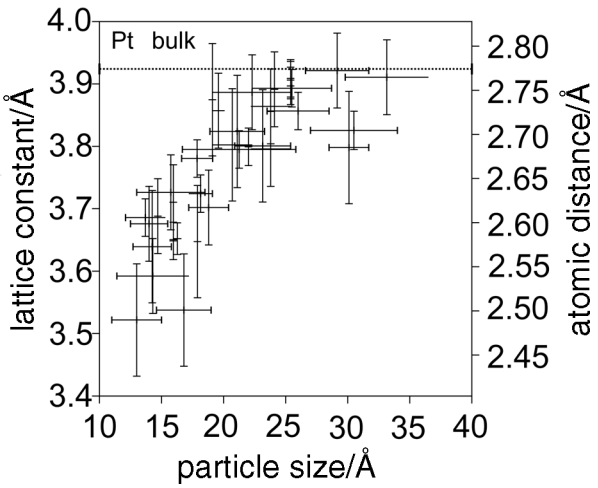

Fig. 21 Lattice constants and interatomic distance of Pt particles grown on Al_2O_3/NiAl(110) as a function of their size (the ends of the horizontal bars represent the width and the length of the particular clusters, respectively, while the vertical bars are error bars).

Of course, the electronic structure of deposited metal aggregates reflects to a certain extent the geometric structure and *vice versa*. The electronic structure, which will be discussed next, has been investigated using various methods including photoemission, X-ray absorption and scanning tunneling microscopy. One particularly interesting aspect in connection with aggregates is the size dependence of the electronic structure in relation with adsorption and reactivity.

Starting from an atomic level diagram, Fig. 22 shows how such a level diagram develops when more and more atoms are agglomerated to form an aggregate and finally a solid with a periodic lattice. Upon formation of an aggregate from equivalent atoms the atomic levels are split into molecular orbitals many of which are degenerate if the symmetry of the system is high. The splittings are characteristic for the intermolecular interactions. Depending on the interaction strength the split levels derived from a given atomic orbital start to energetically overlap with levels derived from other atomic orbitals. As long as the system has molecular character there is an energy gap left between occupied and unoccupied levels, in contrast to the situation encountered for an infinite periodic metallic solid as represented on the right hand side of the figure, where there is no longer a gap between occupied and unoccupied levels. It is not hard to envision now, that as we slowly enlarge the number of atoms in an agglomerate, the gap between occupied and unoccupied orbitals effectively vanishes. It effectively vanishes if the gap energy decreases to a value close to kT. In this situation the changes in the electronic structure would be responsible for an insulator(molecule)–metal transition. The question arises: how many atoms are necessary to induce such a transition? There are several reports in the literature claiming numbers ranging from 20 to several hundred atoms to be necessary.[135,137–149] In this connection, there is one very interesting extrapolation deduced from spectroscopic measurements of the gap of inorganic carbonyl cluster compounds as a function of the metal cluster size. It is shown in Fig. 23[139] and stems from the Longoni group in Bologna. The extrapolation would suggest that 70 atoms are sufficient to close the gap. Comparatively, we have studied deposited clusters of varying size with a combination of photoelectron spectroscopy and X-ray absorption.[141,147,149] Both, the naked as well as the CO covered aggregates, have been studied. Without discussing the results we only state that the extrapolation on the CO covered clusters yields a vanishing gap just below 100 metal

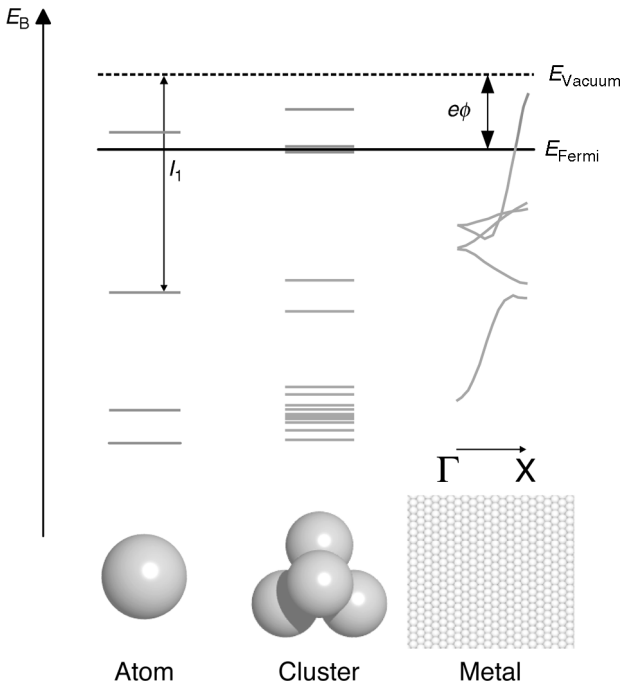

Fig. 22 Diagram illustrating the transition from an atom to a metal. (E_B, binding energy; I_1, first ionisation energy; e, electron charge; ϕ, workfunction; Γ, X, symmetry points in the Brillouin zone.)

atoms. It appears from the STM images that such a situation is reached when the diameter of the aggregate decreases down below 25 Å diameter and a height of 15–20 Å. The aggregate of this size contains 75–100 atoms, a size which well correlates with the extrapolation on the spectroscopic data of carbonyl cluster compounds in Fig. 23, as well as with our results. We take this as a strong indication that at least for the carbon monoxide covered cluster a non-metal-to-metal transition occurs in the vicinity of such a size. Goodman and his group have used scanning tunneling microscopy to investigate the electronic structure of aggregates deposited on oxides.[10,150–152] Fig. 24 shows typical current–voltage curves for some aggregate sizes, *i.e.* Au on TiO_2(110).[150] While the large particles do not exhibit a plateau near $I = V = 0$, the smaller clusters do show the behavior expected for a system with a gap. However, the discrete structures observed for other systems, *i.e.* nanoparticles on graphite[152] and related substrates[153] are not found. The authors report on indications that it is particularly the second layer in the gold aggregates that is responsible for the non-metal-to-metal transition. Au is an interesting low temperature CO oxidation catalyst and the STM findings are important to understand the size specificity of the reaction.

Before we take a closer look at the reactivities of deposited particles we will briefly discuss adsorption properties, as observed mainly through the probe molecule CO. The technique to study CO adsorption is Fourier transform infrared spectroscopy (FTIR) because it provides the resolution to differentiate between various adsorbed species. Again the thin film based systems are particularly well suited because the metallic support of the oxide films acts as a mirror at infrared frequencies. It is, however, also possible to perform such experiments on surfaces of bulk dielectrics as was shown by the Hayden group.[154,155]

Goodman and his group were active in this field early on[152] and have published an interesting study of CO adsorption on Pd aggregates on Al_2O_3 films. The results have been interpreted as characteristic for the adsorption of CO on different facets of the small crystalline aggregates. While this interpretation does not take into account adsorption on the various defect sites of the

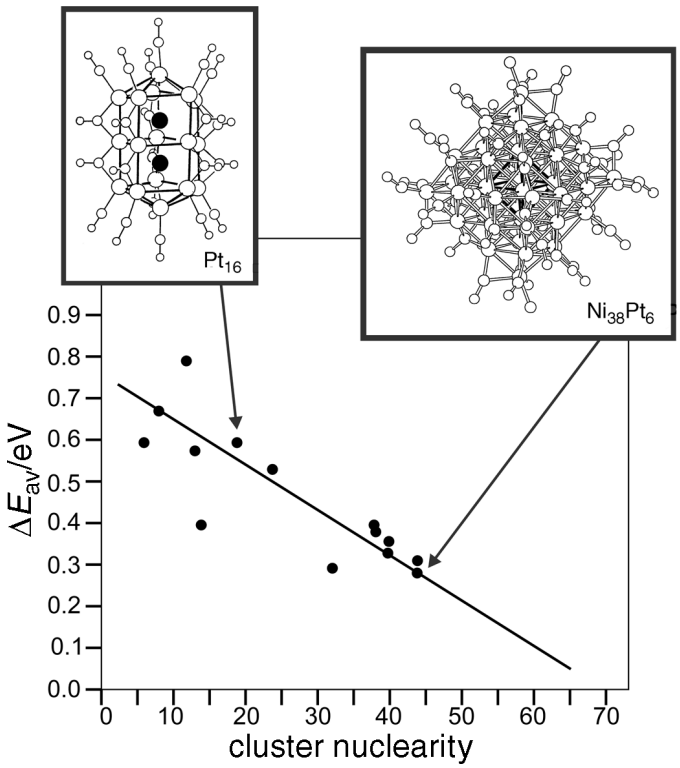

Fig. 23 Electronic excitation of lowest energy for several cluster compounds as a function of metal atoms in the cluster (ΔE_{av} is the energy gap for cluster compounds).

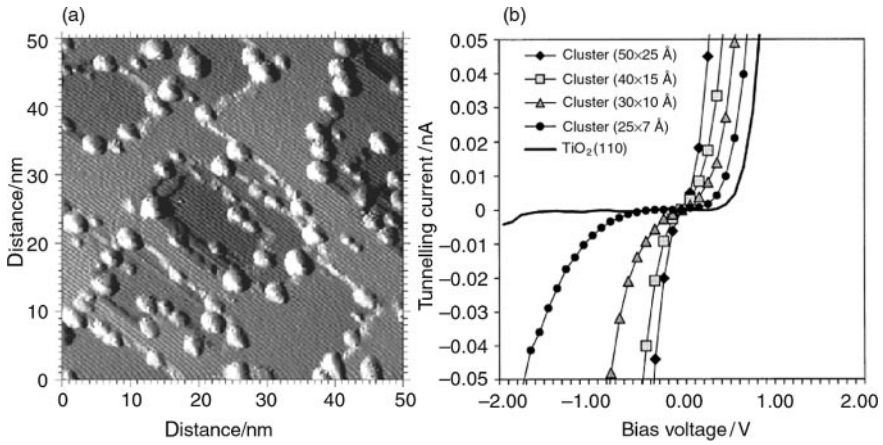

Fig. 24 Current–voltage (b) recorded for Au clusters of various sizes deposited onto a TiO_2(110) surface. A typical STM picture of the system is shown in (a). (Adapted from ref. 151.)

aggregates, which has been pointed out in a more recent study,[156] the data are indicative of the potential of the tool for the study of size dependent absorption studies. We have recently prepared metal deposits on well ordered alumina films at lower temperature including liquid He temperatures, *i.e.* in the range of 50 to 90 K substrate temperature,[157,158] in order to determine the IR characteristics of specific sites.

The infrared spectrum taken from a Rh deposit prepared and saturated with CO at 90 K (average particle size: nine atoms) is displayed in Fig. 25 (left, top corresponding to the spectrum in the middle on the right). The most prominent feature in the stretching region of terminally

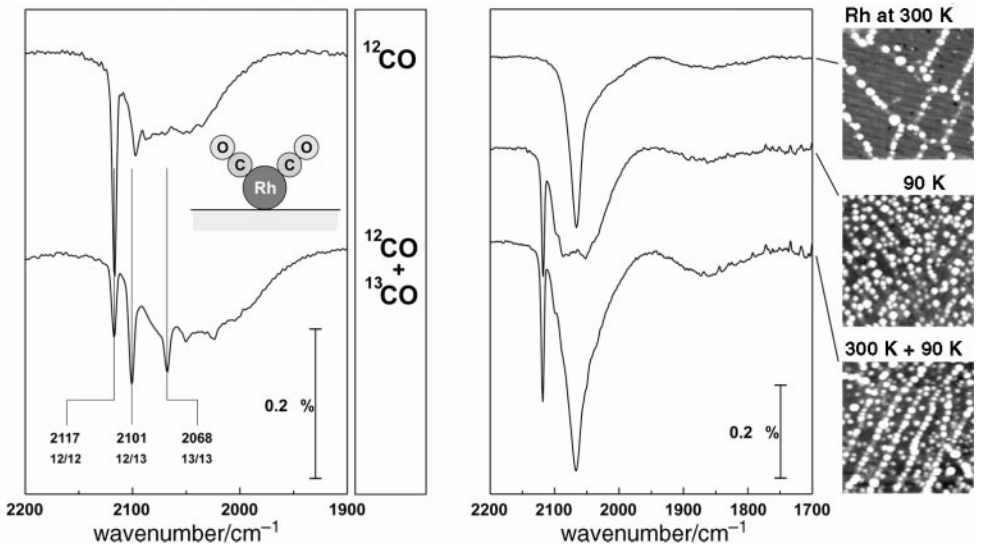

Fig. 25 (Left) Infrared spectra taken after deposition of 0.028 ML Rh on Al_2O_3 and subsequent saturation with ^{12}CO (top) and an approximately equimolar mixture of ^{12}CO and ^{13}CO (bottom) at 90 K. The isotopic compositions giving rise to the three dicarbonyl bands are indicated below the corresponding wavenumbers. Average particle size: nine atoms. (Right) Infrared spectra recorded after CO saturation of Rh deposits at 90 K, along with corresponding room temperature STM images (500 Å × 500 Å). Top: 0.057 ML Rh deposited at 300 K. Middle: 0.057 ML Rh deposited at 90 K. Bottom: 0.057 ML Rh deposited at 300 K, followed by the same exposure at 90 K.

bound CO molecules is a sharp, intense band at 2117 cm^{-1}. This signal has previously been shown to arise from isolated Rh bound to oxide defects.[157] Both the number of adsorbed CO molecules and the nature of the defect site remained unclear. Features at lower frequencies are assigned to molecules on Rh aggregates. In order to get insight into the stoichiometry of the Rh–carbonyl species giving rise to the band at 2117 cm^{-1}, isotopic mixing experiments have been carried out. These experiments allowed us to unambiguously assign this band to a $Rh(CO)_2$ species. Large particles prepared at 300 K deposition temperature, residing on line defects, do not exhibit the $Rh(CO)_2$ band (Fig. 25, right, top spectrum). However, if the spectra are recorded after saturation of the line defects at 300 K, and then further metal is deposited at 90 K (Fig. 25, right bottom spectrum) the $Rh(CO)_2$ band is found, indicating that this species resides in point defect sites. By further reducing the size of the particles we have also identified RhCO and species carrying more than three CO molecules.[158]

In summary, however, we may conclude that several different types of Rh particles are responsible for the observed infrared features. Presently, density functional calculations on small Rh carbonyls are in progress.[159] Calculated vibrational frequencies of such systems may help to identify the species present on the alumina film.

These studies on small Rh particles have been extended to include neighboring elements in the periodic table. Infrared spectra recorded after deposition of comparable amounts of Pd, Rh, and Ir and subsequent CO saturation at 90 K are displayed in Fig. 26. We note differences in the low wavenumber region, where vibrational frequencies of molecules in multiple coordinated sites are located. As on single crystals, the population of such sites is highest on Pd,[160,161] while no such CO is observed on Ir.[162,163]

The differences in the region of terminally bound CO, however, are much more pronounced. In the case of Ir, several distinct features are observed. In analogy to the $Rh(CO)_2$ band at 2117 cm^{-1}, the sharp signal at 2107 cm^{-1} may be attributed to $Ir(CO)_2$ species *via* isotopic mixture experiments (not shown). Bands with similar frequencies have been assigned to the symmetric stretch of $Ir^{+}(CO)_2$ on technical Ir/Al_2O_3 catalysts (2107–2090 cm^{-1})[164] and on the iridium-loaded zeolite H-ZSM-5 (2104 cm^{-1}).[165]

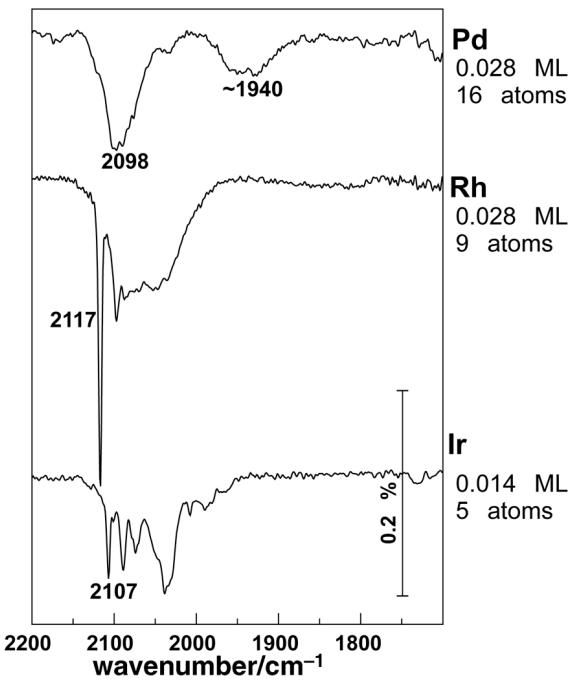

Fig. 26 Infrared spectra of Pd, Ir, and Rh deposited at 90 K and saturated with CO at the same temperature.

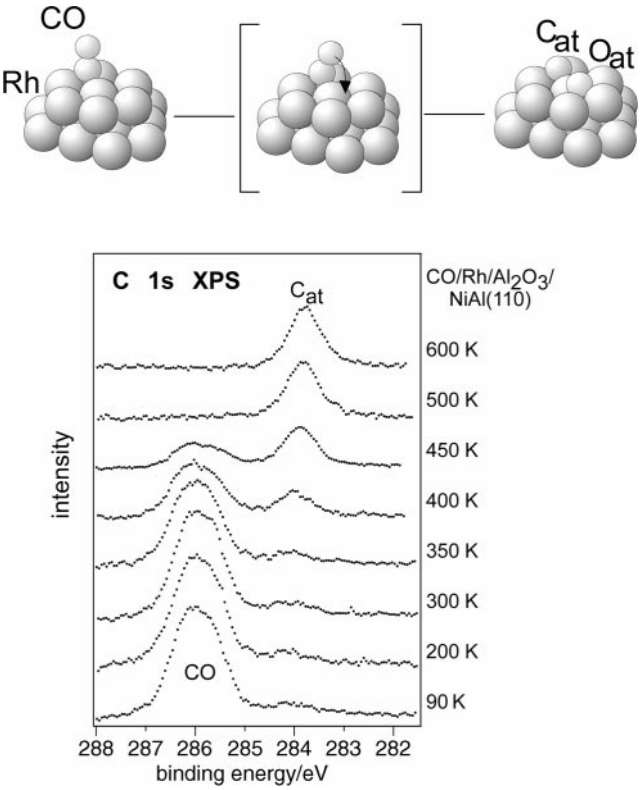

Fig. 27 CO dissociation on $Rh/Al_2O_3/NiAl(110)$: representative series of C 1s spectra taken after CO saturation at 90 K and heating to the indicated temperatures (data acquisition at 90 K).

By contrast, no signs of atomically disperse Pd or of structurally well-defined aggregates are observed. Indeed, the infrared spectrum is rather similar to that observed on much larger, disordered Pd aggregates.[156] At the same metal exposure, the Pd particles are found to be larger than the Rh aggregates by room temperature STM.

Our observations show that infrared spectra of adsorbed CO provide valuable information on the size of metal nanoparticles, as has been long recognized in the catalysis related literature. In the nucleation regime the metal particle size increases from Ir across Rh to Pd, implying the opposite trend in metal oxide interaction strength, *i.e.* Pd < Rh < Ir.

The literature contains several adsorption studies, see for example,[166] employing other probe molecules such as hydrocarbons but here also reaction comes into play which renders the situation even more complicated.

In the following final section several simple chemical reactions of O_2 and CO on small aggregates are addressed.

A simple reaction is the dissociative adsorption of oxygen on small particles. Pd aggregates as shown in Fig. 19 can be imaged at atomic resolution after a dosage to saturation with molecular oxygen from the gas phase.[167] On the side facets the corrugation due to the presence of adsorption of oxygen can be identified. A doubled periodicity corresponding to a $p(2 \times 2)$ structure can be identified. This structure is very similar to the $p(2 \times 2)$ structure observed after dissociative oxygen adsorption on Pd(111).[168] We therefore conclude that a similar situation is encountered in the case of the deposited aggregates. The $p(2 \times 2)$ structure interestingly appears on the different facets at different tunneling conditions. When the oxygen covered Pd aggregates are exposed to carbon monoxide the reactivity of the different facets appear to be different in the sense that the oxygen adsorbate structure is lost on the various facets at variable temperatures and exposures. It will be interesting in the future to study these effects in more detail.

CO oxidation at low temperatures and as a function of size on TiO_2 supported gold aggregates has been studied by the Goodman group.[151] They find a marked size effect of the catalytic activity which correlates with the original observations by the Haruta group[169] for Au on large area titania catalysts. The aggregates near 35 Å size show the maximum activity.

In the future it will be important to perform kinetic measurements for such reactions under well defined conditions including UHV and ambient environments. A very good example has recently been reported by Henry and his group.[170]

Similar to the studies of CO oxidation on Au aggregates reported above, we have undertaken a detailed study of CO dissociation as a function of Rh particle size.[171–173] For various cluster sizes we have taken C 1s photoelectron spectra as a function of sample temperature. An example is shown in Fig. 27 covering a temperature range where we know that the morphology of the ensemble of aggregates does not change. At low temperature the signal typical for molecular CO is observed. Near 400 K a second signal appears indicating the dissociation of CO into carbon and oxygen atoms. At 500 K all molecular CO has been either dissociated or desorbed. The dissociation probability is then given by the relative ratio of the molecular and the atomic C 1s signal. This is plotted in Fig. 28 as a function of the aggregate size. Also included in the figure are data for very small aggregates, where it has been shown that CO dissociation is negligible.[174] This is also true for closed packed single crystal surfaces[175] which would apply to the far end of infinitely large aggregate sizes. If, however, we look at data gained for stepped Rh surfaces then there is a probability for CO dissociation.[176] At an intermediate aggregate size of 200–300 atoms the dissociation probabilities are maximal.

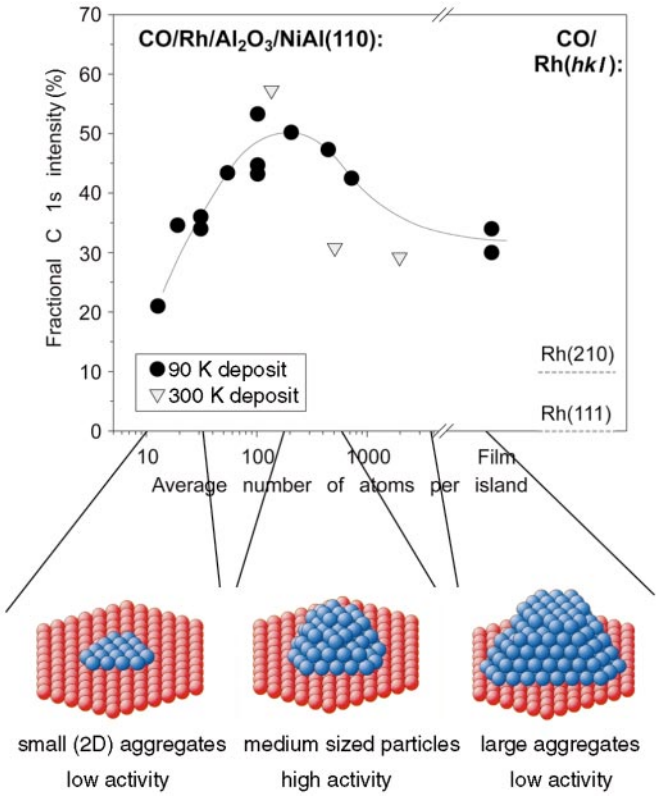

Fig. 28 CO dissociation activity on Rh particles deposited on Al_2O_3/NiAl(110) as determined by XPS. According to ref. 171 and 172 the dissociation activity also passes a maximum for the 300 K deposits, *i.e.* the activity decreases in the regime of small particle sizes reflecting the behavior of the 90 K deposits.

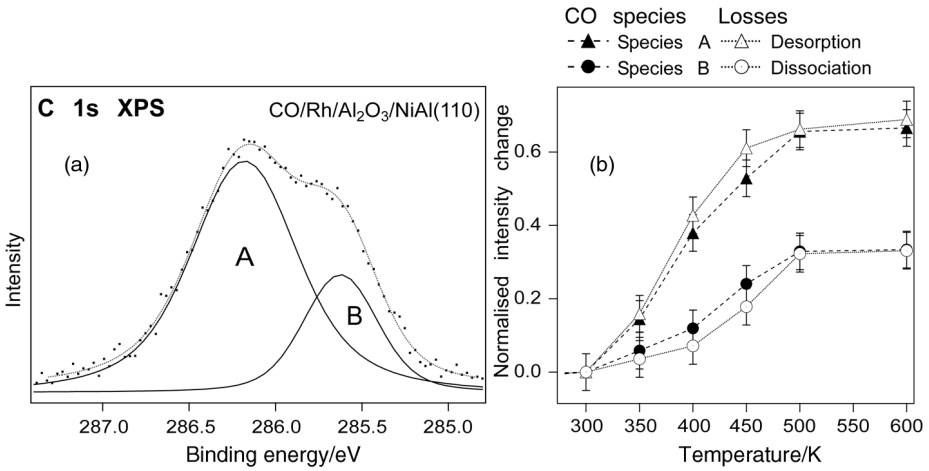

Fig. 29 (a) C 1s spectra of CO adsorbed on Rh particles after saturation at 90 K. (b) Intensity changes for the components A and B as well as the intensity losses due to dissociation and desorption as a function of the annealing temperature (average particle size: $\approx 10^4$ atoms).

Although electronic effects cannot be completely excluded as a reason for the onset of the dissociation phenomenon for small particles, an explanation on the basis of structural properties of the system seems more likely.

Since the Rh deposits are basically disordered, it is easily imaginable that aggregates of medium size exhibit a maximum defect density in terms of steps, kinks and other low coordinate surface atoms. Smaller units should contain less defects, in particular if they are still two-dimensional. In addition to that, spatial constraints may play a role here as well (accommodation of C and O on adjacent sites, see Fig. 27). At high exposures, the step density is reduced due to coalescence processes. For deposition at 300 K, the observed tendency to form crystalline aggregates in the high coverage regime is another factor contributing to a lower defect density. This is consistent with the observation that the dissociation activity declines much faster in this case (see Fig. 28).

An interesting detail concerning the dissociation process has been discovered by a closer inspection of the C 1s emission of the molecularly adsorbed CO.[172] As demonstrated in Fig. 29 (a), the peak actually consists of two components, denoted A and B. If the fraction of the total intensity found for component B after heating to 300 K is compared to the fraction of CO finally dissociating (see Fig. 28), it turns out that the species giving rise to B can be regarded as a kind of dissociation precursor. In fact, the evolution of these two quantities as a function of the particle size is identical, *i.e.* both pass a maximum at the same point.[172] At 90 K, however, this is not yet the case. Here, the relative intensity step which causes a shift of intensity from component A to component B, *i.e.* an increase of the B species which is most pronounced for the medium-sized particles. Interestingly, this conversion is irreversible. Cooling down to 90 K does not lead to an intensity redistribution again.

The conclusion that B is indeed a dissociation precursor is additionally corroborated by Fig. 29 (b) showing the intensity changes for the A and B peaks as well as the losses which result either from desorption or dissociation.[173] Unambiguously, the desorption curve follows the curve for component A, whereas the dissociation curve mimics the development of the component B. Unfortunately, the results allow no further statement as to the nature of the A and B species. It can be assumed, however, that the B species is connected with CO adsorbed on defects. Based on the fact that higher coordinated CO species give rise to lower C 1s binding energies (see above), it may be furthermore speculated whether B is associated with CO in a higher coordination as compared to the A species.

The field of investigations of chemical reactivity as a function of aggregate size is in full development and there are more exciting results at the horizon.

Concluding remarks

After 30 years of surface science, which have seen an enormous development of methods and instrumentation to be applied to the investigation of solid surfaces, the field is now ready to tackle questions of rather complex natures. Naturally, so far metal surfaces have been the focus of attention in surface science and this will continue to be the case. However, also for such systems the complexity of problems is constantly increasing, in particular if molecular adsorbates and self-organized systems are considered. Metal oxide surfaces have received some attention in the recent past and the study of such systems as well as more complex metal–metal-oxide composite systems will, or perhaps has already defined a direction in surface science that promises to reveal interesting results of fundamental interest as well as of appeal towards applications. It is good to see that surface science is very healthy and alive and it has never been farther away from fatality.

I am grateful to my co-workers, present and past, who have contributed to the results presented and whose names appear in the list of references. Also, I am happy to thank many colleagues for stimulating discussions and collaboration. Special thanks go to Ralph Wichtendahl for his help with transparencies and figures.

Over the years many funding agencies and also the private sector have supported our work: Deutsche Forschungsgemeinschaft, Bundesministerium für Bildung und Forschung, Ministerium für Wissenschaft und Forschung des Landes Nordrhein-Westfalen, Fonds der Chemischen Industrie, German–Israeli Foundation, European Union, NEDO International Joint Research Grant on Photon and Electron Controlled Surface Processes, Hoechst Celanese, and Synetix, a member of the ICI group, through their Strategy Research Fund.

References

1 P. A. Cox, *Transition Metal Oxides. An Introduction to their Electronic Structure and Properties*, Clarendon Press, Oxford, 1992.
2 D. A. Johnson, *Some Thermodynamic Aspects of Inorganic Chemistry*, Cambridge University Press, Cambridge, 1982.
3 *Non-stoichiometric Oxides*, ed. O. T. Sorensen, Academic Press, New York, 1981.
4 A. Hamnett and J. B. Goodenough, in *Binary transition metal oxides*, ed. O. Madelung, Springer, 1984.
5 J. F. Owen, K. J. Teegarden and H. R. Shanks, *Phys. Rev. B*, 1978, **18**, 3827.
6 *Surface Science: The First Thirty Years*, ed. C. B. Duke, Elsevier, Amsterdam, 1994.
7 V. E. Henrich and P. A. Cox, *The Surface Science of Metal Oxides*, Cambridge University Press, Cambridge, 1994.
8 C. T. Campbell, *Surf. Sci. Rep.*, 1997, **27**, 1.
9 C. T. Campbell, *Curr. Opin. Solid State Mater. Sci.*, 1998, **3**, 439.
10 D. W. Goodman, *Surf. Rev. Lett.*, 1995, **2**, 9.
11 H.-J. Freund, *Angew. Chem. Int. Ed. Engl.*, 1997, **36**, 452.
12 H.-J. Freund, *Phys. Status Solidi B*, 1995, **192**, 407.
13 H.-J. Freund, H. Kuhlenbeck and V. Staemmler, *Rep. Prog. Phys.*, 1996, **59**, 283.
14 C. R. Henry, *Surf. Sci. Rep.*, 1998, **31**, 231.
15 M. Bäumer and H.-J. Freund, *Prog. Surf. Sci.*, 1999, **61**, 127.
16 J. M. Thomas, *Faraday Discuss.*, 1996, **105**, 1.
17 G. Ertl and H.-J. Freund, *Phys. Today*, 1999, **52**, 32.
18 H. Poppa, *Catal. Rev. Sci. Eng.*, 1993, **35**, 359.
19 U. Diebold, J.-M. Pan and T. E. Madey, *Surf. Sci.*, 1995, **331–333**, 845.
20 G. H. Hardy, *A Mathematician's Apology*, Cambridge University Press, 1940.
21 *Adsorption on Ordered Surfaces of Ionic Solids and Thin Films*, ed. H.-J. Freund and E. Umbach, Springer, Heidelberg, 1993.
22 G. H. Vurens, M. Salmeron and G. A. Somorjai, *Prog. Surf. Sci.*, 1989, **32**, 333.
23 P. L. J. Gunter, J. W. H. Niemantsverdriet, F. H. Ribeiro and G. A. Somorjai, *Catal. Rev. Sci. Eng.*, 1997, **39**, 77.
24 D. A. Bonnell, *Prog. Surf. Sci.*, 1998, **57**, 187.
25 U. Diebold, J. F. Anderson, K.-O. Ng and D. Vanderbilt, *Phys. Rev. Lett.*, 1996, **77**, 1322.
26 P. W. Murray, F. M. Leibsle, C. A. Muryn, H. J. Fisher, C. F. J. Flipse and G. Thornton, *Phys. Rev. Lett.*, 1994, **72**, 689.
27 P. W. Murray, N. G. Condon and G. Thornton, *Phys. Rev. B*, 1995, **51**, 10989.
28 H. Onishi and Y. Iwasawa, *Surf. Sci.*, 1994, **313**, L783.
29 H. Onishi and Y. Iwasawa, *Chem. Phys. Lett.*, 1994, **226**, 111.

30 H. Onishi, K. Fukui and Y. Iwasawa, *Bull. Chem. Soc. Jpn.*, 1995, **68**, 2447.
31 H. Onishi and Y. Iwasawa, *Phys. Rev. Lett.*, 1996, **76**, 791.
32 G. Charlton, P. B. Howes, C. L. Nicklin, P. Steadman, J. S. G. Taylor, C. A. Muryn, S. P. Harte, J. Mercer, R. McGrath, D. Norman, T. S. Turner, and G. Thornton, *Phys. Rev. Lett.*, 1997, **78**, 495.
33 G. Renaud, *Surf. Sci. Rep.*, 1998, **32**, 1.
34 P. W. Tasker, *Adv. Ceram.*, 1984, **10**, 176.
35 W. C. Mackrodt, R. J. Davey, I. N. Black and R. Docherty, *J. Cryst. Growth*, 1987, **82**, 441.
36 C. Noguera, *Physics and Chemistry at Oxide Surfaces*, Cambridge University Press, 1996.
37 P. Guénard, G. Renaud, A. Barbier and M. Gantier-Soyer, *Surf. Rev. Lett.*, 1998, **5**, 321.
38 F. Rohr, M. Bäumer, H.-J. Freund, J. A. Mejias, V. Staemmler, S. Müller, L. Hammer and K. Heinz, *Surf. Sci.*, 1997, **372**, L 291.
39 R. Rohr, M. Bäumer, H.-J. Freund, J. A. Mejias, V. Staemmler, S. Muller, L. Hammer and K. Heinz, *Surf. Sci.*, 1997, **389**, 391.
40 W. Weiss, *Surf. Sci.*, 1997, **377–379**, 943.
41 L. Manassidis and M. J. Gillan, *Surf. Sci.*, 1993, **285**, L517.
42 L. Manassidis and M. J. Gillan, *J. Am. Ceram. Soc.*, 1994, **77**, 335.
43 C. Rebhein, N. M. Harrison and A. Wander, *Phys. Rev. B*, 1996, **54**, 14066.
44 X.-G. Wang, W. Weiss, S. K. Shaikhutdinov, M. Ritter, M. Petersen, F. Wagner, R. Schloegl and M. Scheffler, *Phys. Rev. Lett.*, 1998, **81**, 1038.
45 K. Heinz, *Surf. Sci.*, 1984, **299**, 433.
46 N. M. Harrison, X.-G. Wang, M. Muscat and M. Scheffler, *Faraday Discuss.*, 1999, **114**, 305.
47 H. Schmalzried, *Chemical Kinetics of Solids*, VCH, Weinheim, 1995.
48 D. Wolf, *Phys. Rev. Lett.*, 1992, **68**, 3315.
49 A. Barbier and G. Renauld, *Surf. Sci.*, 1997, **392**, L15.
50 D. Cappus, C. Xu, D. Ehrlich, B. Dillmann, C. A. Ventrice Jr., K. Al-Shamery, H. Kuhlenbeck and H.-J. Freund, *Chem. Phys.*, 1993, **177**, 533.
51 F. Rohr, K. Wirth, J. Libuda, D. Cappus, M. Bäumer and H.-J. Freund, *Surf. Sci.*, 1994, **315**, L977.
52 D. Cappus, M. Hassel, E. Neuhaus, M. Heber, F. Rohr and H.-J. Freund, *Surf. Sci.*, 1995, **337**, 268.
53 A. Barbier, *Proc. 1st Int. Workshop Oxide Surf.* (*IWOX1*), Elmau, Germany, 1999.
54 R. Lacman, *Colloq. Int. CNRS*, 1965, **152**, 195.
55 C. A. Ventrice Jr., T. Bertrams, H. Hannemann, A. Brodde and H. Neddermeyer, *Phys. Rev. B*, 1994, **49**, 1773.
56 A. Barbier, C. Mocuta, H. Kuhlenbeck, K. Peters, B. Richter and G. Renaud, in preparation.
57 W. H. Casey, H. R. Westrich and G. W. Arnold, *Geochim. Cosmochim. Acta*, 1988, **53**, 2795.
58 H. Papp and B. Egersdörfer, personal communication.
59 B. Egersdörfer, PhD Thesis, Bochum, 1993.
60 J. G. Fripiat, A. A. Lucas, J. M. André and E. G. Derouane, *Chem. Phys.*, 1977, **21**, 101.
61 S. Hüfner, P. Steiner, I. Sander, M. Neumann and S. Witzel, *Z. Phys. B*, 1991, **83**, 185.
62 S. Hüfner, *Photoelectron Spectroscopy: Principles and Applications*, Springer-Verlag, Berlin, Heidelberg, 1995.
63 A. Gorschlüter and H. Merz, *Phys. Rev. B*, 1994, **49**, 17293.
64 A. Freitag, V. Staemmler, D. Cappus, C. A. Ventrice, Jr., K. Al-Shamery, H. Kuhlenbeck and H.-J. Freund, *Chem. Phys. Lett.*, 1993, **210**, 10.
65 R. Newman and R. M. Chrenko, *Phys. Rev.*, 1959, **114**, 1507.
66 R. J. Powell, Report no. 5220-1 (unpublished), Stanford Electronics Laboratory, Stanford, 1967.
67 D. Adler and J. Feinleib, *Phys. Rev. B*, 1970, **2**, 3112.
68 B. Fromme, C. Koch, R. Deussen and E. Kisker, *Phys. Rev. Lett.*, 1995, **75**, 693.
69 B. Fromme, M. Möller, T. Anschütz, C. Bethke and E. Kisker, *Phys. Rev. Lett.*, 1996, **77**, 1548.
70 M. Pöhlchen and V. Staemmler, *J. Chem. Phys.*, 1992, **97**, 2583.
71 J. A. Mejias, V. Staemmler and H.-J. Freund, *J. Phys. Condens. Matter*, in press.
72 H. Kuhlenbeck, C. Xu, B. Dillmann, M. Haßel, B. Adam, D. Ehrlich, S. Wohlrab, H.-J. Freund, U. A. Ditzinger, H. Neddermeyer, M. Neuber and M. Neumann, *Ber. Bunsen-ges. Phys. Chem.*, 1992, **96**, 15.
73 C. Xu, B. Dillmann, H. Kuhlenbeck and H.-J. Freund, *Phys. Rev. Lett.*, 1991, **67**, 3551.
74 M. Bender, D. Ehrlich, I. N. Yakovkin, F. Rohr, M. Bäumer, H. Kuhlenbeck, H. J. Freund and V. Staemmler, *J. Phys. Condens. Matter*, 1995, **7**, 5289.
75 M. Henzler and W. Göpel, *Oberflächenphysik des Festkörpers*, Teubner–Verlag, Stuttgart, 1991.
76 K. M. Neyman, G. Pacchioni and N. Rösch, in *Recent Developments and Applications of Modern Density Functional Theory and Computational Chemistry*, ed. J. M. Seminario, Elsevier, Amsterdam, 1996, p. 569.
77 M. Bäumer, J. Libuda and H.-J. Freund, in *Chemisorption and Reactivity on Supported Clusters and Thin Films*, ed. R. M. Lambert and G. Pacchioni, Kluwer Academic Press, Dordrecht, 1997, p. 61.
78 M. A. Nygren and L. G. M. Pettersson, *J. Chem. Phys.*, 1996, **105**, 9339.
79 G. Pacchioni and P. S. Bagus, in *Adsorption on Ordered Surfaces of Ionic Solids and Thin Films*, ed. H.-J. Freund and E. Umbach, Springer Verlag, Berlin, 1993, p. 180.
80 T. Klüner, personal communication.
81 D. Cappus, J. Klinkmann, H. Kuhlenbeck and H.-J. Freund, *Surf. Sci.*, 1995, **325**, L 421.

82 S. M. Vesecky, X. Xu and D. W. Goodman, *J. Vac. Sci. Technol. A*, 1994, **12**, 2114.
83 V. Staemmler, in *Adsorption on Ordered Surfaces of Ionic Solids and Thin Films*, ed. H.-J. Freund and E. Umbach, Springer Verlag, Berlin, 1993, p. 169.
84 M. Pöhlchen, PhD Thesis, Ruhr-Universität, Bochum, 1992.
85 H. Kuhlenbeck, G. Odörfer, R. Jaeger, G. Illing, M. Menges, T. Mull, H.-J. Freund, M. Pöhlchen, V. Staemmler, S. Witzel, C. Scharfschwerdt, K. Wennemann, T. Liedtke and M. Neumann, *Phys. Rev. B*, 1991, **43**, 1969.
86 L. Chen, R. Wu, N. Kioussis and Q. Zhang, *Chem. Phys. Lett*., 1998, **290**, 255.
87 K. M. Neyman, S. P. Ruzankin and N. Rösch, *Chem. Phys. Lett*., 1995, **246**, 546.
88 J.-W. He, C. A. Estrada, J. S. Corneille, M.-C. Wu and D. W. Goodman, *Surf. Sci*., 1992, **261**, 164.
89 S. Furuyama, H. Fuji, M. Kawamura and T. Morimoto, *J. Phys. Chem*., 1978, **82**, 1028.
90 R. Wichtendahl, M. Rodriguez-Rodrigo, U. Härtel, H. Kuhlenbeck and H.-J. Freund, *Phys. Status Solidi A*, 1999, **173**, 93.
91 H. Pfnür, P. Feulner and D. Menzel, *J. Chem. Phys*., 1983, **79**, 4613.
92 C. N. Chittenden, E. D. Pylant, A. L. Schwaner and J. M. White, *Thermal Desorption and Mass Spectrometry*, ed. A. T. Hubbard, CRC Press, Boca Raton, FL, 1995.
93 H. Schlichting and D. Menzel, *Rev. Sci. Instrum*., 1993, **64**, 2013.
94 J. Heidberg, M. Kandel, D. Meine and U. Wildt, *Surf. Sci*., 1995, **333**, 1467.
95 R. Gerlach, A. Glebov, G. Lange, J. P. Toennies and W. Weiss, *Surf. Sci*., 1995, **331–333**, 1490.
96 R. Wichtendahl, PhD Thesis, Freie Universität, Berlin, 1999.
97 M. J. Stirniman, C. Huang, R. C. Smith, J. A. Joyce and B. D. Kay, *J. Chem. Phys*., 1996, **105**, 1295.
98 C. Xu and D. W. Goodman, *Chem. Phys. Lett*., 1997, **L65**, 341.
99 J. Libuda, M. Frank, A. Sandell, S. Andersson, P. A. Brühwiler, M. Bäumer, N. Mårtensson and H.-J. Freund, *Surf. Sci*., 1997, **384**, 106.
100 K. Wolter and M. Frank, personal communication.
101 J. Hemminger, personal communication.
102 R. M. Jaeger, H. Kuhlenbeck, H.-J. Freund, M. Wuttig, W. Hoffmann, R. Franchy and H. Ibach, *Surf. Sci*., 1991, **259**, 235.
103 I. Engquist and B. Liedberg, *J. Phys. Chem*., 1996, **100**, 20089.
104 H. Knözinger and P. Ratnasaniy, *Catal. Rev. Sci. Eng*., 1978, **17**, 31.
105 D. Ehrlich, PhD Thesis, Bochum, 1995.
106 O. Seiferth, K. Wolter, B. Dillmann, G. Klivenyi, H.-J. Freund, D. Scarano and A. Zecchina, *Surf. Sci*., 1999, **421**, 176.
107 A. Zecchina, D. Scarano, S. Bordiga, G. Ricchiardi, G. Spoto and F. Geobaldo, *Catal. Today*, 1996, **27**, 403.
108 C. Xu, M. Haßel, H. Kuhlenbeck and H.-J. Freund, *Surf. Sci*., 1991, **258**, 23.
109 I. Hemmerich, F. Rohr, O. Seiferth, B. Dillmann and H.-J. Freund, *Z. Phys. Chem*., 1997, **202**, 31.
110 P. C. Thüne and J. W. Niemantsverdriet, *Isr. J. Chem*., 1998, **38**, 385.
111 M. Menges, B. Baumeister, K. Al-Shamery, H.-J. Freund, C. Fischer and P. Andresen, *J. Chem. Phys*., 1994, **101(4)**, 3318.
112 I. Beauport, K. Al-Shamery and H.-J. Freund, *Chem. Phys. Lett*., 1996, **256**, 641.
113 T. Klüner, H.-J. Freund, V. Staemmler and R. Kosloff, *Phys. Rev. Lett*., 1998, **80**, 5208.
114 K. Al-Shamery, *Appl. Phys. A*, 1996, **63**, 509.
115 E. A. Wovchko and J. Yates, Jr., *Langmuir*, 1999, **15**, 3506.
116 M. C. Wu and P. J. Møller, *Surf. Sci*., 1989, **221**, 250.
117 P. J. Møller and M. C. Wu, *Surf. Sci*., 1989, **224**, 265.
118 M. C. Wu and P. J. Møller, *Surf. Sci*., 1990, **235**, 228.
119 P. J. Møller and J. Nerlov, *Surf. Sci*., 1993, **307–9**, 591.
120 P. W. Murray, J. Shen, N. G. Condon, S. J. Peng and G. Thornton, *Surf. Sci*., 1997, **380**, L455.
121 P. Stone, R. A. Bennett and M. Bowker, *New J. Phys*., 1998, **1**, 8.
122 U. Diebold, *Proc. 1st Int. Workshop Oxide Surf*. (*IWOX1*), Elmau, Germany, 1999.
123 J. Libuda, F. Winkelmann, M. Bäumer, H.-J. Freund, T. Bertrams, H. Neddermeyer and K. Müller, *Surf. Sci*., 1994, **318**, 61.
124 S. Stempel, M. Bäumer and H.-J. Freund, *Surf. Sci*., 1998, **402–404**, 424.
125 M. Heemeier, PhD Thesis, Berlin, in preparation.
126 T. R. Linderoth, S. Horch, E. Laensgaard, I. Stensgaard and F. Besenbacher, *Surf. Sci*., 1998, **404**, 308.
127 N. Ernst, B. Duncombe, G. Bozdech, M. Naschitzki and H.-J. Freund, *Ultramicroscopy*, 1999, **79**, 231.
128 A. Piednoir, E. Pernot, S. Granjeand, A. Humbert, C. Chapon and C. R. Henry, *Surf. Sci*., 1997, **391**, 19.
129 K. H. Hansen, T. Warren, S. Stempel, E. Laegsgaard, M. Bäumer, H.-J. Freund, F. Besenbacher and I. Stensgaard, *Phys. Rev. Lett*., in the press.
130 M. Methfessel, D. Hennig and M. Scheffler, *Phys. Rev. B*, 1992, **46**, 4816.
131 A. Bogicevic and D. R. Jennison, *Phys. Rev. Lett*., 1999, **82**, 4050.
132 M. Klimenkov, S. Nepijko, H. Kuhlenbeck, M. Bäumer, R. Schlögl and H.-J. Freund, *Surf. Sci*., 1997, **391**, 27.
133 M. Klimenkov, S. Nepijko, H. Kuhlenbeck and H.-J. Freund, *Surf. Sci*., 1997, **385**, 66.

134 S. Nepijko, M. Klimenkov, H. Kuhlenbeck, D. Zemylanov, D. Herein, R. Schlögl and H.-J. Freund, *Surf. Sci.*, 1998, **413**, 192.
135 *Clusters and Colloids: From Theory to Applications*, ed. G. Schmid, VCH, Weinheim, 1994.
136 S. A. Nepijko, M. Klimenkov, M. Adelt, H. Kuhlenbeck, R. Stogl and H.-J. Freund, *Langmuir*, 1999, **15**, 5309.
137 *Metal Clusters*, ed. W. Ekardt, John Wiley, Chichester, 1999.
138 *Transition Metal Clusters*, ed. B. F. G. Johnson, John Wiley, Chichester, 1980.
139 F. F. de Biani, C. Femoni, M. C. Iapalucci, G. Longoni, P. Zanello and A. Ceriotti, *Inorg. Chem.*, 1999, **38**(16), 3721.
140 G. K. Wertheim, S. B. DiCenzo and D. N. E. Buchanan, *Phys. Rev. B*, 1986, **33**, 5384.
141 A. Sandell, J. Libuda, P. Brühwiler, S. Andersson, A. Maxwell, M. Bäumer, N. Mårtensson and H.-J. Freund, *J. Electron Spectrosc. Relat. Phenom.*, 1995, **76**, 301.
142 R. Unwin and A. M. Bradshaw, *Chem. Phys. Lett.*, 1978, **58**, 58.
143 G. K. Wertheim, *Z. Phys. D*, 1989, **12**, 319.
144 S.-T. Lee, G. Apai, M. G. Mason, R. Benbow and Z. Hurych, *Phys. Rev. B*, 1981, **23**, 505.
145 V. de Gouveia, B. Bellamy, Y. Hadj Romdhane, A. Mason and M. Che, *Z. Phys. D*, 1989, **12**, 587.
146 C. Kuhrt and M. Harsdorff, *Surf. Sci.*, 1991, **245**, 173.
147 A. Sandell, J. Libuda, P. A. Brühwiler, S. Andersson, A. J. Maxwell, M. Bäumer, N. Mårtensson and H.-J. Freund, *J. Vac. Sci. Technol. A*, 1996, **14**, 1546.
148 O. D. Häberlen, S.-C. Chung, M. Stener and N. Rösch, *J. Chem. Phys.*, 1997, **106**, 5189.
149 A. Sandell, J. Libuda, P. A. Brühwiler, S. Andersson, M. Bäumer, A. J. Maxwell, N. Mårtensson and H.-J. Freund, *Phys. Rev. B*, 1997, **55**, 7233.
150 D. W. Goodman, *J. Vac. Sci. Technol. A*, 1996, **14**, 1526.
151 M. Valden and D. W. Goodman, *Science*, 1998, **281**, 1647.
152 D. R. Rainer and D. W. Goodman, in *NATO ASI*, ed. G. Pacchioni and R. M. Lambert, Kluwer, Dordrecht, 1997, p. 27.
153 M. Adelt, S. Nepijko, W. Drachsel and H.-J. Freund, *Chem. Phys. Lett.*, 1998, **291**, 425.
154 J. Evans, B. Hayden, F. Mosselman and A. Murray, *Surf. Sci.*, 1992, **279**, L159.
155 J. Evans, B. Hayden, F. Mosselman and A. Murray, *Surf. Sci.*, 1994, **301**, 61.
156 K. Wolter, O. Seiferth, H. Kuhlenbeck, M. Bäumer and H.-J. Freund, *Surf. Sci.*, 1998, **399**, 190.
157 M. Frank, R. Kühnemuth, M. Bäumer and H.-J. Freund, *Surf. Sci.*, 1999, **427**/**428**, 288.
158 M. Frank, R. Kühnemuth, M. Bäumer and H.-J. Freund, *Surf. Sci.*, submitted.
159 T. Mineva and N. Russo, personal communication.
160 P. Uvdal, P.-A. Karlsson, C. Nyberg, S. Andersson and N. V. Richardson, *Surf. Sci.*, 1988, **202**, 167.
161 T. Giessel, O. Schaff, C. J. Hirschmugl, V. Fernandez, K. M. Schindler, A. Theobald, S. Bao, R. Lindsay, W. Berndt, A. M. Bradshaw, C. Baddeley, A. F. Lee, R. M. Lambert and D. P. Woodruff, *Surf. Sci.*, 1998, **406**, 90.
162 G. Kisters, J. G. Chen, S. Lehwald and H. Ibach, *Surf. Sci.*, 1991, **245**, 65.
163 J. Lauterbach, R. W. Boyle, M. Schick, W. J. Mitchell, B. Meng and W. H. Weinberg, *Surf. Sci.*, 1996, **350**, 32.
164 F. Solymosi, É. Novák and A. Molnár, *J. Phys. Chem.*, 1990, **94**, 7250.
165 T. W. Voskobojnikov, E. S. Shpiro, H. Landmesser, N. I. Jaeger and G. Schulz-Ekloff, *J. Mol. Catal. A: Chem.*, 1996, **104**, 299.
166 C. DeLaCruz and N. Sheppard, *J. Chem. Soc. Faraday Trans.*, 1997, **93**, 3569.
167 K. Højrup Hansen, S. Stempel, E. Laegsgaard, M. Bäumer, F. Besenbacher and I. Stensgaard, personal communication.
168 H. Conrad, G. Ertl and J. Küppers, *Surf. Sci.*, 1978, **76**, 323.
169 M. Haruta, *Catal. Today*, 1997, **36**, 153.
170 L. Piccolo, C. Becker and C. R. Henry, *Euro. Phys. J.*, in the press.
171 M. Frank, S. Andersson, J. Libuda, S. Stempel, A. Sandell, B. Brena, A. Giertz, P. A. Brühwiler, M. Bäumer, N. Mårtensson and H.-J. Freund, *Chem. Phys. Lett.*, 1997, **279**, 92.
172 S. Andersson, M. Frank, A. Sandell, A. Giertz, B. Brena, P. A. Brühwiler, N. Mårtensson, J. Libuda, M. Bäumer and H.-J. Freund, *J. Chem. Phys.*, 1998, **108**, 2967.
173 S. Andersson, M. Frank, A. Sandell, J. Libuda, B. Brena, A. Giertz, P. A. Brühwiler, M. Bäumer, N. Mårtensson and H.-J. Freund, *Vacuum*, 1998, **49**, 167.
174 M. P. Irion, personal communication.
175 J. T. Yates, E. D. Williams and W. H. Weinberg, *Surf. Sci.*, 1980, **91**, 562.
176 M. Rebholz, R. Prins and N. Kruse, *Surf. Sci.*, 1991, **259**, L791.
177 K. Refson, R. A. Wogelius, D. G. Fraser, M. C. Payne, M. H. Lee and V. Milman, *Phys. Rev. B*, 1995, **52**, 10823.
178 U. Birkenheuer, J. C. Boettger and N. Rösch, *J. Chem. Phys.*, 1994, **100**, 6826.
179 P. A. Redhead, *Vacuum*, 1962, **12**, 203.

Paper 9/07182B